OceanMesh2D 1.0: MATLAB-based software for two-dimensional unstructured mesh generation in coastal ocean modeling

Keith J. Roberts[1], William J. Pringle[1], and Joannes J. Westerink[1]

[1]Department of Civil and Environmental Engineering and Earth Sciences, University of Notre Dame, 156 Fitzpatrick Hall, Notre Dame, IN

Correspondence: Keith J. Roberts (krober10@nd.edu)

Abstract. OceanMesh2D is a set of user-friendly MATLAB functions with pre- and post-processing utilities to generate two-dimensional (2D) unstructured meshes for coastal ocean circulation models. These meshes are generated according to a variety of feature driven geometric and topo-bathymetric mesh size functions, which are controlled by user-defined parameters. Mesh generation is achieved through a force-balance algorithm to locate vertices and a number of topological improvement strate-
5 gies aimed at improving the worst case triangle quality and adjusting the shoreline representation. The software embeds the mesh generation process into an object-orientated framework that facilitates rapid workflows on personal computers. These workflows are flexible, reproducible, and script-able. Through real world examples, we illustrate the various capabilities of the software and demonstrate how it can produce high-quality, multiscale, unstructured meshes that are faithful to a variety of constraints and automatically conform to arbitrary shoreline vector datasets. The objective of this paper is to describe the
10 functionality of the software.

1 Introduction

Many applications in the coastal ocean may be accurately modeled by the shallow-water equations such as the astronomical tides, tsunamis, and storm surges. Unstructured meshes are often used for numerical simulations of coastal ocean circulation because they can naturally resolve the large range of length scales necessary for accurate hydrodynamic predictions and conform
15 well to complicated shoreline boundaries. The accuracy and the associated computational expense of the mesh are in direct conflict, which makes the mesh design process challenging. Computational work is governed by the distribution of vertices (mesh resolution) and accuracy is determined, in part, by the representation of relevant geometrical and bathymetric features that may influence the simulation of the shallow-water physics. Due to this balance between accuracy and computational work, the prescription of the mesh resolution often leads to a highly subjective and non-reproducible mesh generation process. To
20 address this issue, the ocean modeling community has developed approaches and tools to build unstructured meshes for coastal circulation problems (Hagen et al., 2002; Bilgili et al., 2006; Gorman et al., 2006, 2008; Lambrechts et al., 2008; Conroy et al., 2012; Engwirda, 2017; Candy and Pietrzak, 2018). Most works have either tried to minimize topo-bathymetric interpolation error on the mesh (e.g., Gorman et al., 2008), or construct the mesh based on resolving relevant physical processes in the domain and/or preserving the geometry of the boundary (e.g., Conroy et al., 2012; Engwirda, 2017). An iterative *a posteriori*

method which aims to keep the local truncation error constant throughout the mesh has also been employed (Hagen et al., 2002).

Often mesh generators are written in languages like C or C++ and use expert language and complex mathematical ideas, which may require a steep-learning curve to operate the software and can be challenging to adapt to the user's needs. In contrast, modern scripting based programming environments such as MATLAB and Python are attractive to many users because they are simpler to modify and include a plethora of built-in or community developed functions, toolboxes and packages that are freely available. For instance, a simple and easily adaptable mesh generator based on the concept of force equilibrium and written in a few dozen MATLAB lines is *DistMesh* (Persson and Strang, 2004). The simplicity of the force-equilibrium algorithm makes it attractive as a general-purpose mesh generator by allowing users and developers to adapt it for various applications (e.g., Engsig-Karup et al., 2008; Liu, 2009; Nguyen et al., 2010; Wang et al., 2014). However, due to the general nature of *DistMesh*, it tends to be computationally inefficient for the large and highly multi-scale geophysical domains encountered in coastal ocean hydrodynamic modeling problems. Additionally, there are a number of pre- and post-processing steps that must be performed to prepare the geospatial data for meshing and operate on the mesh so that it is amenable for numerical simulation. For instance, one must obtain a shoreline boundary that will lead to a mesh that is practical to simulate with. By integrating the tools to pre-process the geospatial data into the mesh generator directly, it reduces the time spent performing these essential tasks and performs the process in a self-consistent, reproducible way.

In a related previous work, the Advanced Mesh generator (ADMESH; Conroy et al., 2012) implemented a *DistMesh* based coastal ocean mesh generator in MATLAB. In this work, we build and improve on many of the ideas described in ADMESH with the following primary improvements: a) a focus on computational efficiency to enable the MATLAB paradigm to become practically achievable even for exceedingly large geophysical datasets, b) inclusion of pre- and post-processing workflows, c) a greater variety of mesh size functions and flexibility in their application which offers more control over mesh resolution placement, and critically: d) transparent, flexible and adaptable code written in an open-source environment for the benefit of the community. The codes place emphasis on facilitating reproducible mesh design workflows that lead to the creation of the meshes and also the necessary model inputs for a numerical simulation following many of the ideas described in Candy and Pietrzak (2018). These mesh generation workflows (i.e., a user-specified MATLAB control script) are typically represented by a few lines of formulaic MATLAB code and take between minutes to an hour to generate relatively large, multiscale, high-fidelity meshes and their auxiliary components completely automatically on a personal computer.

The software is written in an object-orientated framework that is divided into a set of standalone classes (Table 1) related to: 1) processing geospatial datasets used in the mesh generation process; 2) computing mesh size functions; 3) performing the mesh generation; 4) storing, visualizing, and post-processing the mesh output. Special attention has been made to ensure that paid MATLAB toolboxes are not required to generate a mesh. Further, in its current state the software contains a number of post-processing functions specific to the ADvanced CIRCulation model (ADCIRC; Luettich and Westerink, 2004), but these can be naturally adapted to other solvers in the future. The rest of this paper is structured as follows: we begin by introducing the framework and organization of the code, followed by a detailed description of each of the four standalone classes. In order to demonstrate certain aspects of the classes a few meshing examples are illustrated. This includes real world examples in

Table 1. Classes in OceanMesh2D

Class name	Purpose
geodata	Process geospatial data: mesh boundaries (e.g. coastline) & digital elevation data
edgefx	Compute the mesh size functions based on geospatial data and parameters.
meshgen	Mesh generator + descriptor for parameters and geospatial data used in generation process to build mesh.
msh	Store and visualize mesh topology and associated attributes.

Jamaica Bay, New York (JBAY), Galveston Bay, Houston (GBAY), and the western Atlantic Ocean with focused refinement around Puerto Rico and the U.S. Virgin Islands (PRVI) (see Table 2 for details of the various options/parameters and datasets used to generate these example meshes).

2 Coding framework

5 The automated generation of geophysical-use unstructured meshes often requires a number of user defined parameters and a variety of geospatial data as inputs. The resulting mesh is related to the algorithms and data that were used to create it. These task- and object- specific properties of the mesh generation process provide the motivation behind the development of an object-orientated programming (OOP) approach since data and the methods used are tightly coupled together in OOP (Register, 2017). In this software, the use of OOP is not only to encourage mesh portability and reproducibility but also to

10 promote organized workflows.

OceanMesh2D is composed of four classes (*geodata*, *edgefx*, *mshgen*, and *msh*, see Table 1 for a brief description of each class) and a utilities directory containing various standalone functions. The *geodata* class is used as a preprocessor to mesh generation and creates an appropriate meshing boundary from user-supplied inputs. The *edgefx* class enables the user to build mesh size functions with a variety of different options and constraints. The *mshgen* and *msh* class are associated with mesh

15 generation and inherit various options from the *geodata* and *edgefx* classes. These four classes are constructors for creating specific instances of each class otherwise known as objects. All classes are activated through the use of name-value pairs where the "name" represents an option and the "value" is the parameter relevant to that option. The following sections will detail each class and its various methods. Additional technical information can be found in the user guide (Roberts and Pringle, 2018).

Although each individual class is standalone, there exists a specific workflow that is typically followed to build coastal ocean

20 meshes with this software (Fig. 1). In this workflow, each object is passed to the subsequent constructor that inherits various properties of the previous object (in addition to other user-defined parameters unique to that constructor). As demonstrated in section 5.2, the structure of this workflow allows the user to create numerous instances of the *geodata* and *edgefx* classes that can be simultaneously passed to the *meshgen* class. This can be used to seamlessly mesh high resolution insets contained within wider coverage geospatial data that are associated with coarser mesh size functions. This use case is regarded as particularly

25 useful and pragmatic given the finite computational memory and the sparse coverage and heterogeneous resolution of publicly available high-resolution bathymetric data.

Table 2. Datasets and parameters used to generate the example meshes for this paper and which are released with the toolkit. The final mesh quality and the number of iterations in the mesh generator to achieve this are also noted.

Region	Data sources	bbox	h0 (m)	Meshing Parameters hmax (m)	α_R	α_{wl}	α_{slp}	α_g	α_{ch}	Δ_t (s)	Mesh Quality $\overline{q_E}$	q_{Emin}	Iterations $\ni q_{L3\sigma} > 0.75$
JBAY	NCEI Post-Sandy (1/9 arc-sec DEM)[1]	[-73.97 -73.75 40.50 40.68]	15	1,000	3	–	–	0.15	–	2	0.97	0.60	38
GBAY	Galveston (1/3 arc-sec DEM)[2]	[-95.40 -94.40 29.14 30.09]	60	1,000	3	–	–	0.25	0.10	–	0.97	0.53	71
PRVI	GSHHS_f_L1 (ESRI Shapefile coastline)[3] SRTM15_PLUS (15 arc-sec DEM)[4]	[-100 -53 5 52.5]	1,000	10,000	5	30	15	0.25	-	0**	0.97	0.45	30
	Puerto Rico (1 arc-sec DEM)[2]	DEM*	30										
	U.S. Virgin Islands (1 arc-sec DEM)[2]	DEM*	30										
	San Juan (1/9 arc-sec DEM)[2]	DEM*	10										

*: The bbox is set to that of the DEM extents

**: Setting $\Delta t = 0$ invokes the automatic time step selector option (see section 4.6)

1 Eakins et al. (2015); available from https://www.ngdc.noaa.gov/mgg/inundation/sandy/sandy_geoc.html

2 Eakins and Taylor (2010); available from https://ngdc.noaa.gov/mgg/coastal/coastal.html

3 Wessel and Smith (1996); available from http://www.soest.hawaii.edu/pwessel/gshhg/

4 Becker et al. (2009); available from ftp://topex.ucsd.edu/pub/srtm15_plus/
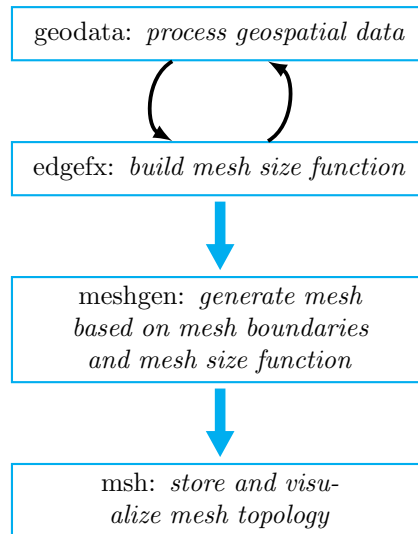
Figure 1. Standard workflow used to build meshes with OceanMesh2D. The black arrows indicate that these steps can be repeated in a loop over many datasets.

2.1 Workflow provenance and mesh container: *msh* class

It is often difficult, if not impossible, to reproduce the element connectivity since the geospatial data used to define the mesh domain and the description of how resolution is distributed is often not stored with the mesh (Candy and Pietrzak, 2018). A scripting-based approach forces the user to create an input file with the options, parameters, and geospatial data used in the

5 mesh generation process. Thus, since the mesh can be built on any machine nearly identically, we envision that the script file used to build the mesh can be simply provided as supplementary material with any related published work in order to promote reproducibility and transparency.

To store the triangulation and related files, we have created a data structure called a *msh* object. A *msh* object is a data storage class that contains triangulation-related attributes and support for solver-specific input files. The format of the *msh*

10 class uses MATLAB's dot-structure syntax that naturally enables option-hierarchy, organizes the numerous associated data files in one place, and simplifies the interaction with the underlying data by creating a set of standardized methods (Table 3). Upon termination of the mesh generator, a *msh* class object containing the triangulation is returned and can be saved efficiently to hard disk as a MATLAB .mat file.

While the underlying purpose of the *msh* class is to store the mesh data, the OOP framework enables specific methods

15 to be associated with the class. This enables the *msh* class to act as an intermediary between the numerical solver and the user to assist the creation of solver-specific files and perform common data-driven operations on the mesh. For instance, there are a set of procedures that must be applied to a mesh to ensure it's suitable for numerical simulation such as renumbering the vertices, visual inspection of the mesh connectivity, topo-bathymetric interpolation, boundary condition application, and control file generation (see Table 3 for the complete list of *msh* methods). Rather than have each user independently write their

Table 3. Select methods of the *msh* class and from the utilities directory*

Method	Purpose
msh	Creates an empty *msh* class or reads ADCIRC 'fort.##' file(s) into a *msh* class.
write	Writes out populated objects inside the *msh* class into ADCIRC 'fort.##' file(s).
plot	Visualize various properties of the mesh such as the triangulation, bathymetry, resolution, slope, and boundary condition types.
renum	Renumber the mesh to minimize the element bandwidth using Reverse Cuthill-McKee.
interp	Interpolate gridded topo-bathymetric data and its gradient onto the mesh.
makens	Applies boundary condition types (what ADCIRC calls 'nodestrings').
plus; +	Add (merge) two meshes together using Boywer-Watson incremental triangulation and local smoothing.
minus; −	Removes the intersection of two meshes from the first mesh
CalcCFL	Calculates Cr (17) based on a certain Δt, or determines the maximum allowable Δt at each vertex given the constraint $Cr < 1$.
CheckTimestep	Decimates vertices in the mesh so that the constraint $Cr < 1$ is satisfied for a given Δt
reconstructEdgefx	Make a structured grid mesh size function based on the mesh resolution
baryc	Get the element barycenters
bound_con_int	Bound the mesh's vertex connectivity following Massey (2015)
flipEdge	Flip the edge of a triangle.
extdom_polygon	Walk and record the polygonal boundaries of the mesh
extdom_edges	Calculate the boundary edges of the mesh.
extdom_boundary	"Walk" a boundary segment given the start and endpoint vertex.
VertToVert	Calculate the vertex connectivity of the mesh.
SmoothMesh	Apply Laplacian smoothing to mesh.

*There are a number of other standalone functions contained with the 'utilities' directory that perform operations on the *msh* class but which are not dynamic methods of this class

own methods to accomplish these tasks, we believe it to be more advantageous to place these static or dynamic methods inside the *msh* class that can be edited by everyone using a version control software.

3 Geospatial data: *geodata* class

The *geodata* class is a preprocessor to the mesh generator. It is used to create an appropriate mesh boundary description from user supplied input files. The *geodata* class also stores the region of the digital elevation model (DEM) that overlaps with the desired meshing domain efficiently in memory. This DEM data is used in the construction and computation of a number of mesh size functions (see *edgefx* class) and *msh* methods.

The discrete representation of the boundary is a critical step in ocean modeling applications. A common problem with defining a mesh boundary along a highly irregular, fractal shoreline is that it may require unfeasibly small mesh resolution to correctly capture its complexity. To tackle this problem, a number of works have developed shoreline simplification algorithms to rearrange mesh boundary vertices so to balance the accuracy of the discrete shoreline given the user requested mesh resolution (e.g., Gorman et al., 2008; Candy et al., 2014; Candy and Pietrzak, 2018). In this work, through the adoption of the

DistMesh algorithm, we avoid this issue by automatically resolving or de-resolving the shoreline via the mesh size function and a series of post-processing steps. The post-processing steps remove regions of the mesh that are invalid as a result of inadequately prescribed resolution in the vicinity of shoreline complexities. The end result is a mesh boundary that is simplified to closely match the desired mesh size function without the need to edit the shoreline beforehand. These post-processing steps

5   will be explained in Sect. 5.1.

3.1   Projections

Users often want an ability to bound mesh resolution sizes in certain parts of a large coastal modeling domain. In order to accurately enforce these constraints, a projection from the spherical geometry of the Earth to a planar one $\mathbb{R}^3 \rightarrow \mathbb{R}^2$ is necessary. In this software, the mesh is generated and output in the World Geographic Coordinate System (WGS84); therefore,

10   all geospatial data must be supplied in this geographical coordinate system. For the formation of some mesh size functions that rely on bathymetric gradients and distances, we use a simple relationship between WGS84 degrees and planar meters to calculate the underlying grid spacing:

$$\delta_{lon}^* = \delta_{lon}\frac{\pi R_E}{180}cos\phi, \qquad \delta_{lat}^* = \delta_{lat}\frac{\pi R_E}{180} \tag{1}$$

where δ_{lon} and δ_{lat} define the DEM resolution in WGS84 degrees between meridians and parallels, respectively, R_E is the

15   mean radius of the Earth (≈ 6378 km), δ_{lon}^* and δ_{lat}^* are the distances between meridians and parallels in meters, and ϕ is the latitude in radians. To enforce mesh resolution constraints, we use the Haversine formula to convert between WGS84 and meters. An assumption is made that the length in geographic degrees forms a horizontal (i.e., latitude parallel) edge starting at the point it is defined at. The distance between the start and end point of this edge are converted to Great Circle distances using the Haversine method and then, later, we invert the Haversine formula and solve for WGS84 degrees by assuming that

20   the distance between latitudes is zero:

$$h_d = 2\arcsin\left(\sec\phi\sin\left(\frac{h^*}{2R_E}\right)\right) \tag{2}$$

where h^* is the length of the edge in meters, and h_d is the length of the edge in WGS84 degrees. The assumption that the edgelength extrudes along a latitude parallel is reasonable in practice because the mesh size function constraints matter mostly in areas of relatively high mesh refinement and, in these locations, the variation in ϕ is small.

25   ### 3.2   Mesh boundary definition and shoreline data

Since a coastline is often approximated by a series of piecewise linear segments, the mesh boundary is often unbounded on the ocean-side. Thus, the user often has to turn their segments that represent the shoreline into a closed polygon for any meshing algorithm to work properly. To make this process self-consistent and automatic, we allow the user to specify the meshing region

as a rectangular *bbox*.

$$bbox = [x_0, y_0] \times [x_1, y_1] \tag{3}$$

where x_0, y_0 are the geographic coordinates of the bottom-left corner and x_1, y_1 are the the geographic coordinates of the top-right corner.

5   The boundary of the meshing domain is implicitly defined through the use of a signed distance function (Persson and Strang, 2004). Let Ω be a planar subset of $\mathbb{R}^2$ and a shoreline polygon be a piecewise straight line graph composed of a set of vertices $S = (s_1, s_2, ..., s_N)$ listed in consecutive order in which $s_1 = s_N$, otherwise $s_i \neq s_j, \forall i = 1, N$. A segment is then defined as a line composed of two consecutive vertices $\in S$. The area enclosed by S is denoted as $\mathcal{S}$ and the area enclosed by *bbox* is denoted as $\mathcal{B}$. The mesh domain is defined as an area Ω through the intersection of $\mathcal{S}$ and $\mathcal{B}$.

$$\Omega = \mathcal{S} \cap \mathcal{B} \tag{4}$$

Within Ω, the signed distance d is defined as a mapping $d_\Omega : \mathbb{R}^2 \to \mathbb{R}$

$$d(\boldsymbol{x})_\Omega = s_\Omega(\boldsymbol{x}) \min_{\boldsymbol{y} \in \partial\Omega} (||\boldsymbol{x} - \boldsymbol{y}||) \tag{5}$$

where $|| \cdot ||$ is the standard Euclidean norm in $\mathbb{R}^2$ (i.e., the distance to the boundary of the meshing domain), $\boldsymbol{x}, \boldsymbol{y}$ are points, and the sign function s_Ω is given by:

$$s(\boldsymbol{x})_\Omega := \begin{cases} -1, & \text{if } \boldsymbol{x} \in \Omega. \\ +1, & \text{if } \boldsymbol{x} \in \mathbb{R}^2 \setminus \Omega. \end{cases} \tag{6}$$

If $\boldsymbol{x}$ lies within Ω, then $d(\boldsymbol{x})$ will be negative. It follows from the above:

$$\begin{aligned} \Omega &:= \left\{ \boldsymbol{x} \in \mathbb{R}^2 : d(\boldsymbol{x})_\Omega \leq 0 \right. \\ \partial\Omega &:= \left\{ \boldsymbol{x} \in \mathbb{R}^2 : d(\boldsymbol{x})_\Omega = 0 \right. \end{aligned} \tag{7}$$

In addition to defining $\partial\Omega$, the signed distance function is used to form mesh size functions (see Sect. 4) and during the execution of the meshing algorithm. The signed distance is computed through a combination of the MATLAB class version (Bagon, 2009) of the Approximate Nearest Neighbor (ANN) method (Arya and Mount, 1993; Mount and Arya, 2006) (to obtain the absolute distance), and Dr. Darren Engwirda's points-in-polygon test (*inpoly.m*; available from https://www.mathworks.com/matlabcentral/fileexchange/10391-fast-points-in-polygon-test) function (to get the sign). The ANN

method has high computational efficiency with a negligible memory footprint in comparison to the *dsegment.m* function available in *DistMesh*, and *inpoly.m* is several hundred-fold quicker ($O(\log N)$ vs. $O(n^2)$) than MATLAB's built-in *inpolygon.m*.

In our methodology, the shoreline polygon is internally partitioned into mainland and island polygons (this categorization is defined below). New vertices are added to the shoreline polygon so that it conforms to the user-requested minimum mesh resolution ($h0$) inside *bbox*. Further, vertices are decimated outside *bbox* to save both memory and time during the mesh generation process since the calculation of Eq. (5) is proportional to the number of shoreline vertices.

1. The segments of S that intersect with $\mathcal{B}$ are read in to memory.

2. The segments of S are classified into three types: mainland, inner, or outer.

    (a) The mainland category contains segments that are not totally enclosed inside the $\mathcal{B}$.

    (b) The inner (i.e., islands) category contains polygons totally enclosed inside the $\mathcal{B}$.

    (c) The outer category is the union of the mainland, inner, and $\mathcal{B}$.

3. New vertices are added on these segments so that no two consecutive vertices along it are further than $\frac{h0}{2}$. This is necessary for accurate re-projection of points that exit the meshing domain during the execution of the *DistMesh* algorithm (Persson and Strang, 2004).

4. All segments are smoothed using a n-point moving average. Simultaneously, small islands that have an area less than $(p * h0)^2$ are removed where n and p are user-specified integers ($n = 5$, $p = 4$ by default).

As an example, the following steps are applied to a shoreline extracted from a NCEI Post-Sandy DEM (source listed in Table 2) leading to a classification of shoreline points that is crucial for correct automatic meshing of the complicated coastal domain it describes without human intervention (Fig. 2).

Perhaps the most accurate *global* shoreline database suitable for automatic mesh generation is the Global Self-consistent Hierarchical High-resolution Shorelines (GSHHS) (Wessel and Smith, 1996). This database is guaranteed to not have any coastlines that self-intersect and it has a resolution of about 50-m in most areas, which makes it useful for the generation of greater than approximately 100-m minimum resolution meshes. However, for meshes with a desired resolution finer than 100-m or so, the GSHHS is largely insufficient as it often misses critical connections between water bodies that are far finer than 50-m (Fig. 3). A more accurate representation of the meshing domain can often be obtained by extracting a geometric contour that represents the topo-bathymetric height (e.g., 0-m, 5-m, 10-m) above a datum from a DEM. By utilizing a geometric contour, the resulting shoreline boundary in the mesh will be fully consistent with the topo-bathymetric data, which we find can be helpful in producing stable meshes. However, a geometric contour extracted directly from a gridded dataset may not be a polygon by default and may contain breaks or gaps. If the vector shoreline data is not a polygon, we have included a *geodata* method 'close' that implements a flood-fill algorithm in order to obtain a suitable polygonal boundary for our software. The implementation is borrowed from Dr. Darren Engwirda's JIGSAW-GEO package (Engwirda, 2017). Artificial gaps in the contour that may originate from noise in the DEM can be largely eliminated by using the r.contour module in GRASS GIS
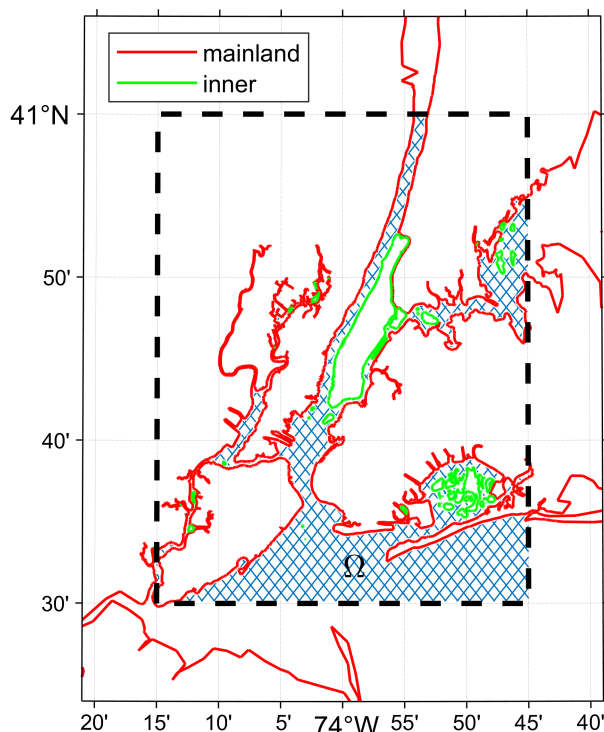
Figure 2. Example of boundary treatment in and around New York, United States; the *bbox* is indicated by the thick dashed black line, the meshing region Ω is hatched in blue, and the categorization of land boundary types are indicated according to the colored lines.

(GRASS Development Team, 2017) with a cut parameter generally between 50 and 200. See the User Guide (Roberts and Pringle, 2018) for more details on these aspects of creating self-consistent coastlines.

4   Automatic mesh size function: *edgefx* class

The careful placement of mesh resolution is critical to create meshes that lead to accurate but efficient simulations. There are

5   a number of heuristics used to design unstructured meshes for shallow-water flow applications. A review of some common resolution heuristics utilized in coastal ocean modeling can be found in Greenberg et al. (2007). We have considered a variety of constraints involved in the formation of the mesh size functions by integrating and adapting past work on the topic. The various mesh size functions are detailed in this section.

Mesh resolution is distributed in the domain according to a mesh size function. The mesh size functions $h(\boldsymbol{X}) : \mathbb{R} \rightarrow \mathbb{R}$ are

10   constructed on a *structured* grid that relates every point in Ω to a desired mesh size h, or more precisely, a triangular edgelength (hence *edgefx*). There are many techniques to form mesh size functions that vary principally around the methodology to form the background grid on which the mesh sizes are calculated (Persson, 2006). For example, the simplest approach is to use a Cartesian or structured grid for the mesh size function. A structured grid has some advantages over an unstructured one related
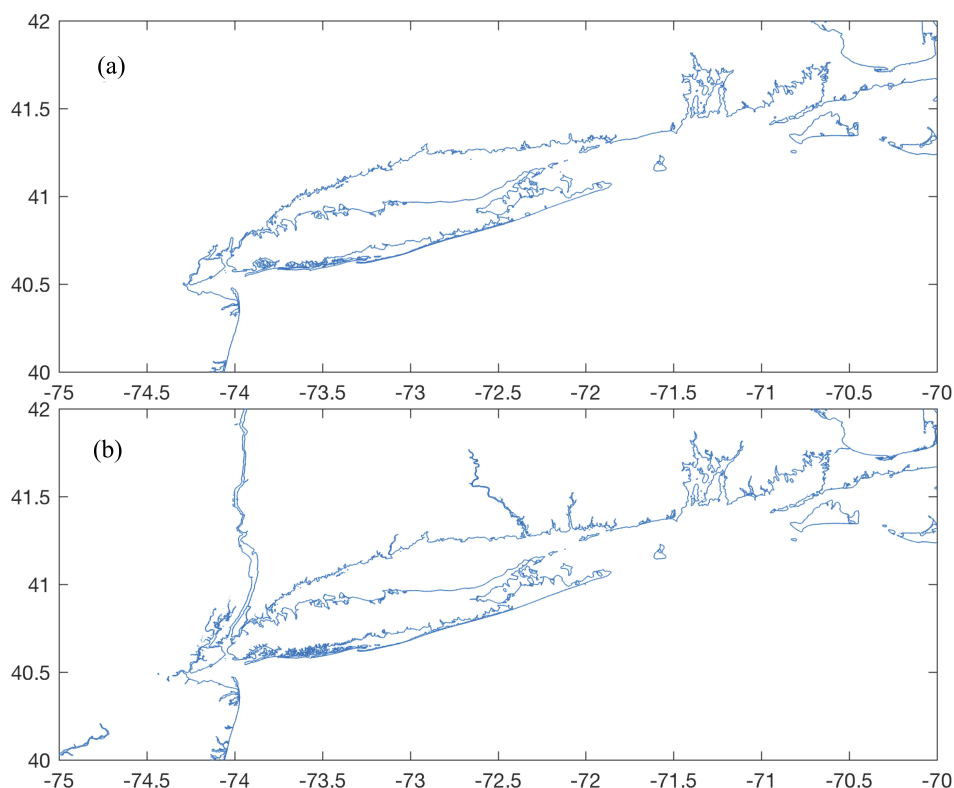
Figure 3. (a) The GSHHS fine (i.e., GSHHS_f) shoreline centered around New York, United States; (b) a shoreline extracted from mosaicing NCEI Post-Sandy LiDAR tiles with the GRASS GIS software.

to computational efficiency when storing, querying, interpolating, and performing calculations. Further, bathymetric data is often defined on structured grids, and in these cases, it makes sense to compute the mesh size function directly on the same grid to minimize interpolation error. Given these reasons, we calculate our mesh size functions on Cartesian grids defined in geographical coordinates (i.e., WGS84). A major drawback to this approach is that the entire domain must be uniformly refined which becomes particularly severe for relatively large meshing domains. This impacts the scalability of the subsequent mesh generation process. We present a solution to this problem in Sect. 5.2.

The function $h(\boldsymbol{X})$ is finalized by taking the minimum of the potentially multiple mesh size functions and applying, if specified, user defined minimum and maximum bounds on mesh resolution in meters that can be specified within depth ranges. Each individual mesh size function is based on either shoreline data and/or the bathymetric data passed to the *edgefx* class constructor. Currently, the software supports a variety of mesh size functions that are used in the ocean modeling community: wavelength-to-grid-size (Westerink et al., 1994; Luettich and Westerink, 2013), topographic length scale (Greenberg et al., 2007; Lambrechts et al., 2008), Euclidean distance from the shoreline (Persson and Strang, 2004), approximate feature size of the shoreline (Persson, 2006; Koko, 2015), thalweg/polyline (Heinzer et al., 2012), and Courant-Friedrichs-Lewey (CFL)-limiting (Bilgili et al., 2006). Each mesh size function can either be incorporated or omitted based on the user's requirements.

Finally, $h(\boldsymbol{X})$ is graded using a marching algorithm (Persson, 2006) to ensure that the triangle-to-triangle change in edgelength is bounded below a user-defined percent, α_g. The *limgradStruct.m* function that performs this grading has been specially modified for the structured grid mesh size functions used in this software.

4.1 Distance and feature size

5   A high degree of refinement is often necessary near the mesh boundary $\partial\Omega$ to capture the geometric complexity of the shoreline. If mesh resolution is poorly distributed, critical conveyances may be missed leading to larger scale errors in the nearshore circulation (Greenberg et al., 2007). Thus, a mesh size function that is equal to a user-defined minimum mesh size $h0$ along $\partial\Omega$ and grows as a linear function of distance d from the nearest $\partial\Omega$ point may be appropriate:

$$h_{dis} = h0 - \alpha_d d \tag{8}$$

10   where α_d is the percent change of mesh size with distance from S. Eq. (8) is what we call the *distance* mesh size function, and is originally presented in the *DistMesh* algorithm (Persson and Strang, 2004).

One major drawback of the *distance* mesh size function is that the minimum mesh size will be placed even along straight stretches of coastline. If this is undesirable, a *feature* mesh size function that places resolution according to the geometric width of the coastline should instead be employed (Conroy et al., 2012; Koko, 2015). In this function, the feature size (e.g., the width

15   of channels/tributaries, and the radius of curvature of the shoreline) along the coast is estimated by computing distances to the medial axis of the shoreline geometry. Here we have implemented an approximate medial axis method closely following Koko (2015). This involves finding local extrema in the gradient of the d, which in practice, amounts to defining a medial point as a location where $||\nabla d|| < 0.9$ and $d < 0$ (Koko, 2015). Sometimes due to the configuration of the mesh size function grid juxtaposed on the shoreline geometry, medial points inside small channels may be aliased. These medial points can be

20   recovered by classifying mesh size function grid points as medial points if their neighbors are outside of the domain but the mesh size function point under question is within the domain. Once the medial points are computed, the local feature size h_{lfs} is calculated as:

$$h_{lfs} = \frac{2(d_{MA} - d)}{\alpha_R} \tag{9}$$

where α_R is the user specified number of desired elements per local feature size (commonly $3 \leq \alpha_R \leq 6$), and d_{MA} is the

25   absolute distance to the nearest medial point. Since the medial axis is an approximation, the identification of the full set of medial points depends on the horizontal resolution of the mesh size function. This implies that the *feature* mesh size calculation will work best when computed on a structured grid of resolution similar of finer than the horizontal resolution of the supplied geophysical data.

To demonstrate the efficacy of the *feature* mesh size function, we use a 1/9 arc second (approximately 3-m) LiDAR topo-

30   bathy DEM (Table 2) to generate an approximate 10-m minimum element size mesh of Jamaica Bay in New York, United
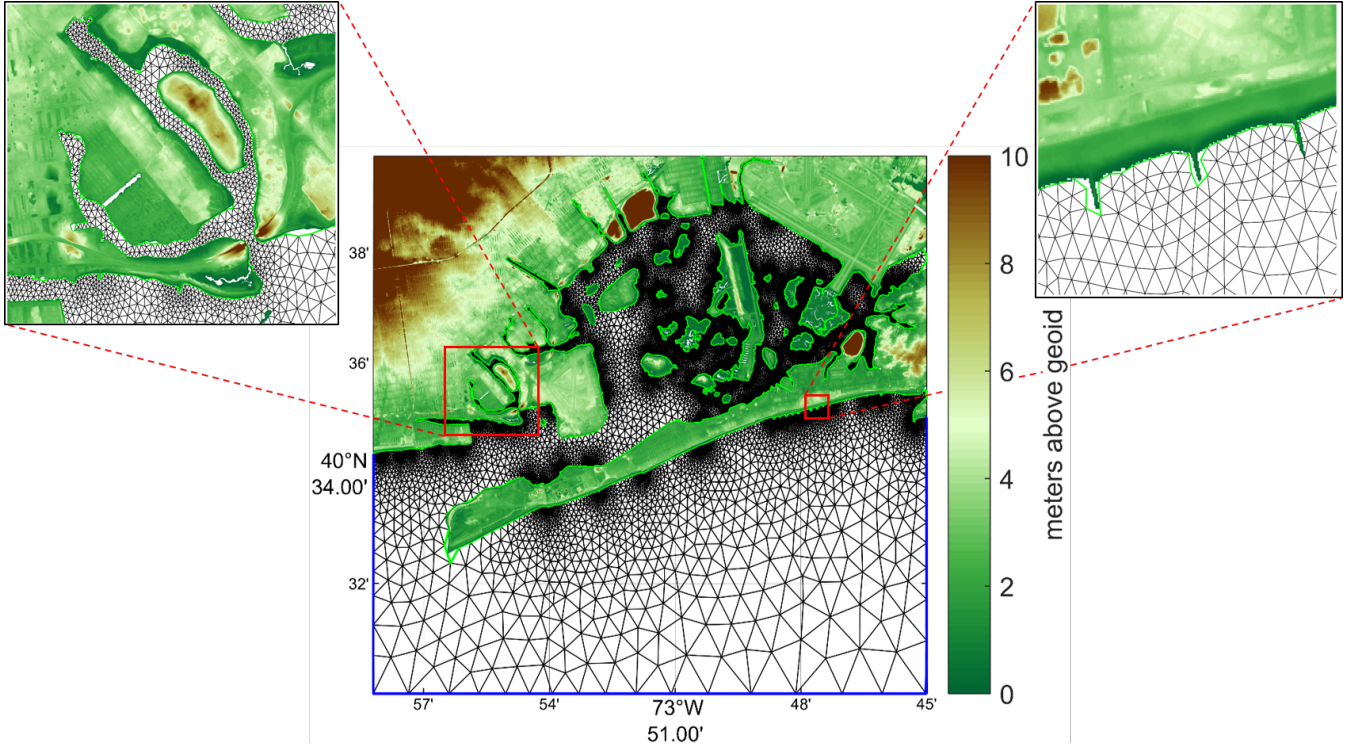
Figure 4. Mesh connectivity in and around Jamaica Bay, New York built using the JBAY example script. Closeup views of two regions highlight how the *feature* mesh size function automatically places higher resolution through constrictions (left) and around coastal groin structures (right). The NCEI Post-Sandy DEM heights above the geoid are plotted in overland regions.

States (Fig. 4), with $\alpha_R = 3$. Relatively coarse resolution is placed along linear regions of the sand bar, while the dark patches indicate where higher resolution is automatically placed around points of high curvature in the coastline and through channels. For example, two closeups are shown where higher resolution is placed along a narrow constriction and around perpendicular coastal groins along a beach.

5   **4.2   Grading and mesh size interactions**

It is necessary to ensure a size smoothness limit α_g such that for any two adjacent vertices $\boldsymbol{x_i}$, $\boldsymbol{x_j}$ connected by an edge, the local increase in mesh size is bounded above such that:

$$h(\boldsymbol{x_j}) \leq h(\boldsymbol{x_i}) + \alpha_g ||\boldsymbol{x_i} - \boldsymbol{x_j}|| \tag{10}$$

A smoothness criteria is essential to produce a mesh that can simulate physical processes with a practical time step as sharp gra-

10   dients in mesh resolution typically lead to triangles with highly skewed angles inevitably resulting in poor numerical accuracy (Shewchuk, 2002). We adopt a marching method to smooth $h(\boldsymbol{X})$ originally proposed by Persson (2006) and later adapted by

Engwirda (2014, 2017) that preserves gradients well. We have further adapted this algorithm for support on structured grids in MATLAB (implemented in *limgradStruct.m* function). In general, a smoother edgelength function is congruent with a higher overall triangle quality but with more triangles in the mesh. Generally, setting $0.2 \leq \alpha_g \leq 0.3$ produces good results without over-resolving the mesh. It is important to note that the rate of mesh resolution increase is bounded above by the grade; there-

5   fore, if the distance parameter in Eq. (8) is set to a value lower than the grade ($\alpha_d < \alpha_g$), then grading should have no effect on the mesh size function.

Here we demonstrate the relative effects of the *distance* and *feature* mesh size functions and their interaction with the grade. To illustrate this, a mesh is created over an estuary-like geometry with *distance* ($\alpha_d = 0.15$ and $\alpha_d = 0.35$) and *feature* ($\alpha_R = 3$ and $\alpha_R = 6$) mesh size functions, each using two different grading parameters ($\alpha_g = 0.15$ and $\alpha_g = 0.35$) (Fig. 5).

10 The *distance* mesh size function focuses resolution on the mesh boundary, which is often not necessary to resolve areas that are geometrically simple. Further, the use of a *distance* mesh size function often results in comparatively larger triangles in the center of the geometry; especially with a relatively high grade (i.e., 35%; Fig. 5d). In shallow estuaries, this can be undesirable as the bathymetric representation of high conveyance channels in the center of the estuary will be inaccurate, aliasing the transported mass and energy. In contrast, the *feature* mesh size function tries to place a uniform number of triangles across the

15 widest axis of the feature (Fig. 5e,f). It focuses mesh resolution on regions that are narrow and/or where the shoreline has high curvature. The net result is a comparatively smaller number of vertices than the *distance* mesh size function (for $\alpha_R < 20$ in this example). Depending on the selection of α_R in the local feature size equation Eq. (9), the size of the mesh resolution in the center of the estuary can be bounded even when using a relatively high mesh grade ($\alpha_g > 0.25$). This is advantageous because a higher grade can dramatically lower the overall vertex count. Conversely, a relatively low grade ($\alpha_g < 0.20$) can hinder the

20 *feature* mesh size function from expanding efficiently, and may be somewhat counter-productive to its purpose.

4.3   Wavelength

In shallow water theory, the wave celerity, and hence the wavelength λ, is proportional to the square-root of the depth of the water column. This relationship indicates that more mesh resolution at shallower depths is required to resolve waves that are shorter than those in deep water. With this considered, a mesh size function h_{wl} that ensures a certain number of elements are

25 present per wavelength (usually of the M_2 dominant semi-diurnal tidal species) can be deduced:

$$h_{wl} = \frac{\lambda_{M2}}{\alpha_{wl}} \tag{11}$$

$$h_{wl} = \frac{T_{M2}}{\alpha_{wl}}\sqrt{gb} \tag{12}$$

where λ_{M2} and T_{M2} are the wavelength and period ($\approx$12.42 hours) of the M_2 tidal wave, g is the acceleration due to Earth's gravity, b is the bathymetric depth, and α_{wl} is the user specified number of elements chosen to resolve the wavelength. If

30 the M_2 wavelength is sufficiently captured, the diurnal species will also be sufficiently resolved since their wavelengths are approximately twice as large as the M_2. In general, the wavelength parameter α_{wl} is set to a value somewhere between 25 and 100 (Westerink et al., 1994; Le Provost and Lyard, 1997).
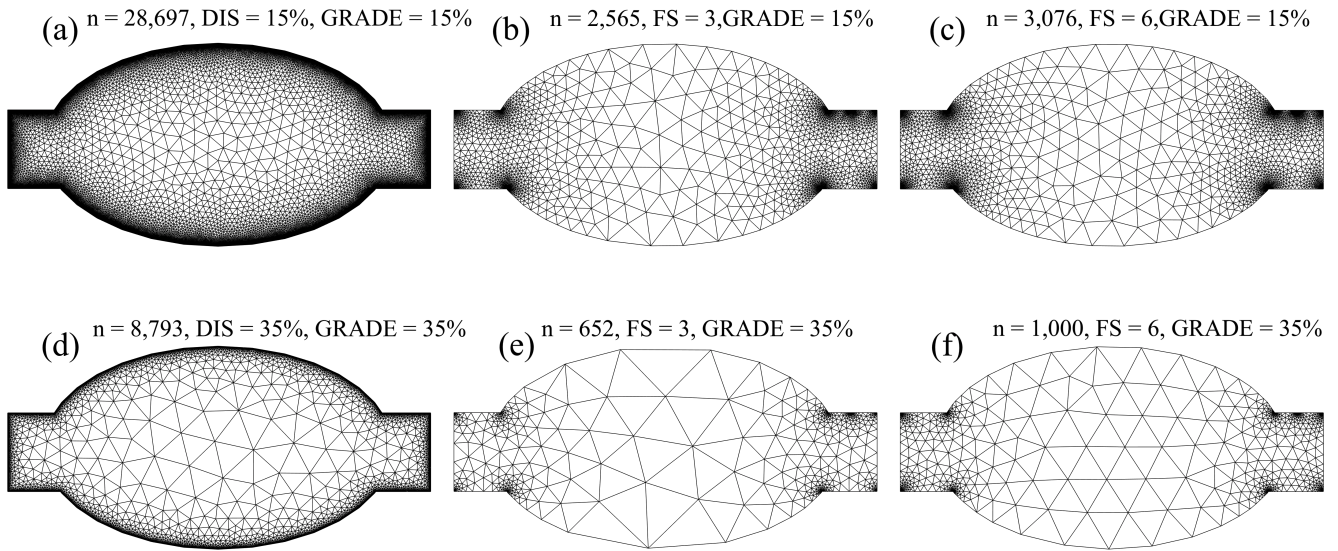
Figure 5. Depiction of mesh resolution interactions between the grade (α_g), *distance* (DIS), and *feature* (FS) mesh size functions. Panels a-c depict the resolution with a grade equal to 15% (α_g = 0.15), panels d-f with a grade equal to 35% (α_g = 0.35). The first column depicts how mesh resolution is distributed with a *distance* mesh size function and the second and third columns show how the mesh size varies with the *feature* mesh size function with α_R equal to 3 and 6, respectively. In the title of each panel, the number of vertices n in the triangulation is shown.

4.4 Topographic length scale

Large mesh resolution can emerge in deeper waters with just the usage of the distance, feature size, and/or wavelength mesh size functions. Larger mesh resolution in deeper waters can lead to under resolving the sharp topographic gradients that characterize the continental shelf break. These slope features can be important for coastal ocean models in order to capture dissipative effects driven by the internal tides, transmissional reflection at the shelf break that control the astronomical tides, and trapped shelf waves (Huthnance, 1995). The scaling of the slope parameter, commonly called the topographic length scale, is usually represented by the following:

$$h_{slp} = \frac{2\pi}{\alpha_{slp}} \frac{b}{|\nabla b|} \tag{13}$$

where $2\pi/\alpha_{slp}$ is the number of elements that resolve the topographic slope, and ∇b is the gradient of the bathymetry evaluated on a structured grid of horizontal resolution $h0$. The 2π factor is a convention introduced by Lyard et al. (2006) so that α_{slp} can be set to a value similar in magnitude to α_{wl}, e.g. around 10-30.

Typically the gradient of the bathymetry often contains a high degree of noise, which results in high mesh refinement with the application of h_{slp} despite the fact that small features have marginal effects on shallow water flow, particularly in deep water (LeBlond, 1991). We would like to filter bathymetric features that are not relevant to the underlying shallow-water processes,
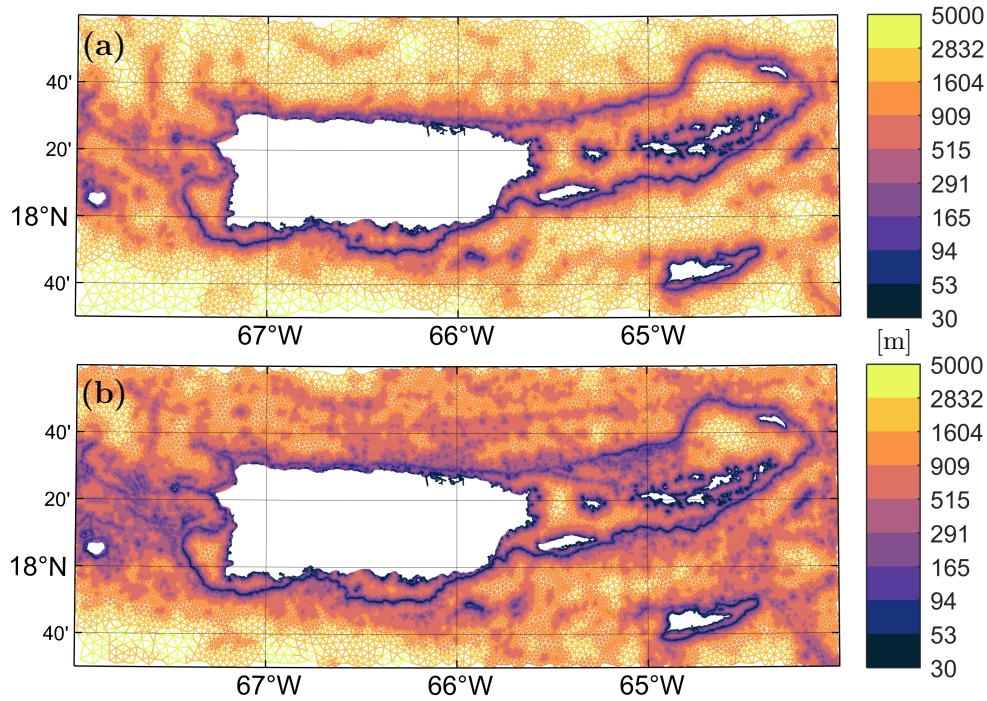
Figure 6. Local mesh resolution (defined as the local element circumradius [m]) in the PRVI example (see Table 2) around the Puerto Rico and U.S. Virgin Island inset region, with (a) and without (b) the Rossby radius slope filter applied. The 'thermal' color palette from cmocean (Thyng et al., 2016) is used in this figure.

like the astronomical tides. Therefore, we low-pass filter the bathymetry before calculating the gradient by default. In this low-pass filter, we propose a filter cutoff based on an estimate of the *local* Rossby radius of deformation:

$$L_R = \frac{\sqrt{gb}}{f} \tag{14}$$

where f is the Coriolis force. By *local* we mean that we discretely bin values of L_R in Ω and apply a low-pass filter to those
5   binned grid points with a cutoff set to L_R at the bin midpoint. For this approach to work correctly, partitioning the meshing domain is critical because Ω can often span large regions of latitude with highly varying f. Here, the PRVI example (see Table 2 and Sect. 5.2 for more details on this example) is used to demonstrate the effect of the Rossby radius slope filter (Fig. 6). The mesh with the Rossby radius slope filter focuses mesh resolution at large and relatively shallow features such as the continental shelf break, and avoids the placement of resolution over deep and small scale features that are not comparable to L_R. As a
10   result, the filtered mesh has 27% fewer vertices in the illustrated region.

4.5 Channel Thalwegs/Polylines

Closer to the shoreline, the width of the nearshore geometry through which water must flow eventually becomes the dominant length scale instead of L_R. Thus, constraints imposed by continuity normally become more important than dynamic balances in determining spatial scales in the estuary (LeBlond, 1991). Following this logic, the representation of the cross-sectional area

5   of the channel that connects the ocean to the estuary is critical in order to simulate an accurate exchange of water.

The predominant conveyance through a watercourse is often is approximated by a series of neighboring points that connect local minimums in bathymetric depth. These locations are referred to collectively as a thalweg and are represented as polylines in the GIS framework. The level of mesh refinement near and around the thalweg can affect the bathymetric representation in the mesh through aliasing local minimums in bathymetric depth. Often the associated length scale of these features is too small

10   to successfully resolve through the topographic length scale mesh size function, so instead we propose a mesh size function similar to the feature size constraint function proposed by Heinzer et al. (2012). The purpose of this mesh size function is to locally enhance mesh refinement around thalwegs that would otherwise be under-resolved with the previously proposed mesh size functions (e.g., the wavelength mesh size function which would reduce mesh resolution along a deep-draft channel).

Thalwegs can be located by thresholding upslope area (O'Callaghan and Mark, 1984) using a DEM along with GIS software

15   such as GRASS. One difficulty with thresholding upslope area to identify submerged channels is that it may produce spurious non-physical channel networks, especially in areas of flat bathymetry. GIS software like GRASS allow for interaction with this vector data and it is encouraged to utilize modules within the GIS software framework (e.g., r.stream.extract, v.stream.network) to ensure that the network is accurate before meshing.

This mesh size function treats the thalwegs as a set of connected vertices that form polylines and operates only the polylines

20   that intersect with the $bbox$ polygon. This mesh size function distributes resolution as follows:

1. A circular region in the mesh size function is formed on each thalweg point with a diameter, dia, equal to:

$$dia = 2b\tan(\theta) \tag{15}$$

where θ is the angle of reslope.

2. In each circular region, the mesh size function is assigned resolution by

25    $$h_{ch} = \frac{b}{\alpha_{ch}} \tag{16}$$

This assumes the thalweg has a cross-sectional area that resembles a v-shape with a bank angle of θ (which is set to $60°$ by default) and that the stencil becomes larger as the b increases. (Fig. 7).

As the water column deepens, the horizontal length scale greatly enlarges, which implies that the dynamical effects from small-scale features like thalwegs should weaken. This dynamic is qualitatively captured through Eq. (15) by the enlargement

30   of the region the thalweg effects in the mesh size function as the water depth increases. Additionally, the quotient α_{ch} in
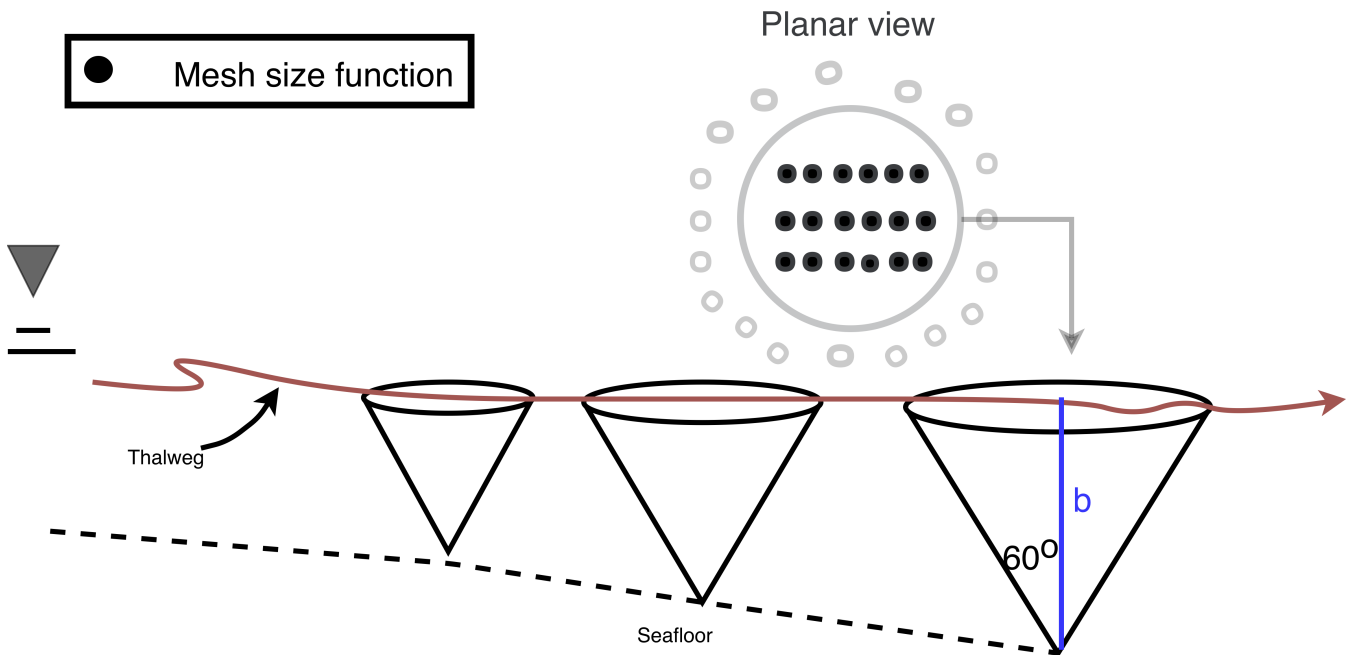
Figure 7. A schematic illustrating various aspects of the channel mesh size function. The thalweg is depicted as the maroon line. Along some points along thalweg, cones are drawn to depict the regions inside the mesh size function where the mesh size function is altered.

Eq. (16) alters how the resolution scales with bathymetric depth to further reflect the fact that the horizontal length scale tends to grow as the water becomes substantially deeper, thus reducing the resolution around thalwegs.

As an example of this mesh size function, a mesh is built in and around Galveston Bay (GBAY; Table 2). Galveston Bay, located in the vicinity of Houston, Texas, is a shallow-estuary with a heavily trafficked shipping channel along its centerline. In this example, we have provided the thalweg points by thresholding the Galveston DEM (Table 2) with an upslope area of 10,000 cells using GRASS GIS. Visually, the mesh generated using the channel mesh size function clearly captures the bathymetric feature of the Houston Shipping channel to a higher-degree of accuracy (Fig. 8). Without the use of this mesh size function, the model design would be forced to use an extremely high degree of refinement everywhere to capture the Houston ship Channel and its adjacent features, or hand-edit the mesh resolution, which, in both cases, are inefficient methodologies.

4.6 Courant-Friedrichs-Lewey (CFL)-Limiting

The computational expense of a computational model and associated code is significantly affected by the time step that must be used to ensure stability and accuracy. For models that use explicit time stepping schemes, a necessary condition for numerical stability is determined by the Courant-Friedrichs-Lewey (CFL) condition. Although this is not a sufficient condition, it is a practical way to gauge the success of a new mesh. The CFL condition states that the Courant number (Cr) must be less than or equal to 1. Stricter conditions may be relevant for different numerical schemes and due to nonlinearities in the governing equations and the amount (Brufau et al., 2004). Additionally, the accuracy of a numerical scheme is also impacted by the
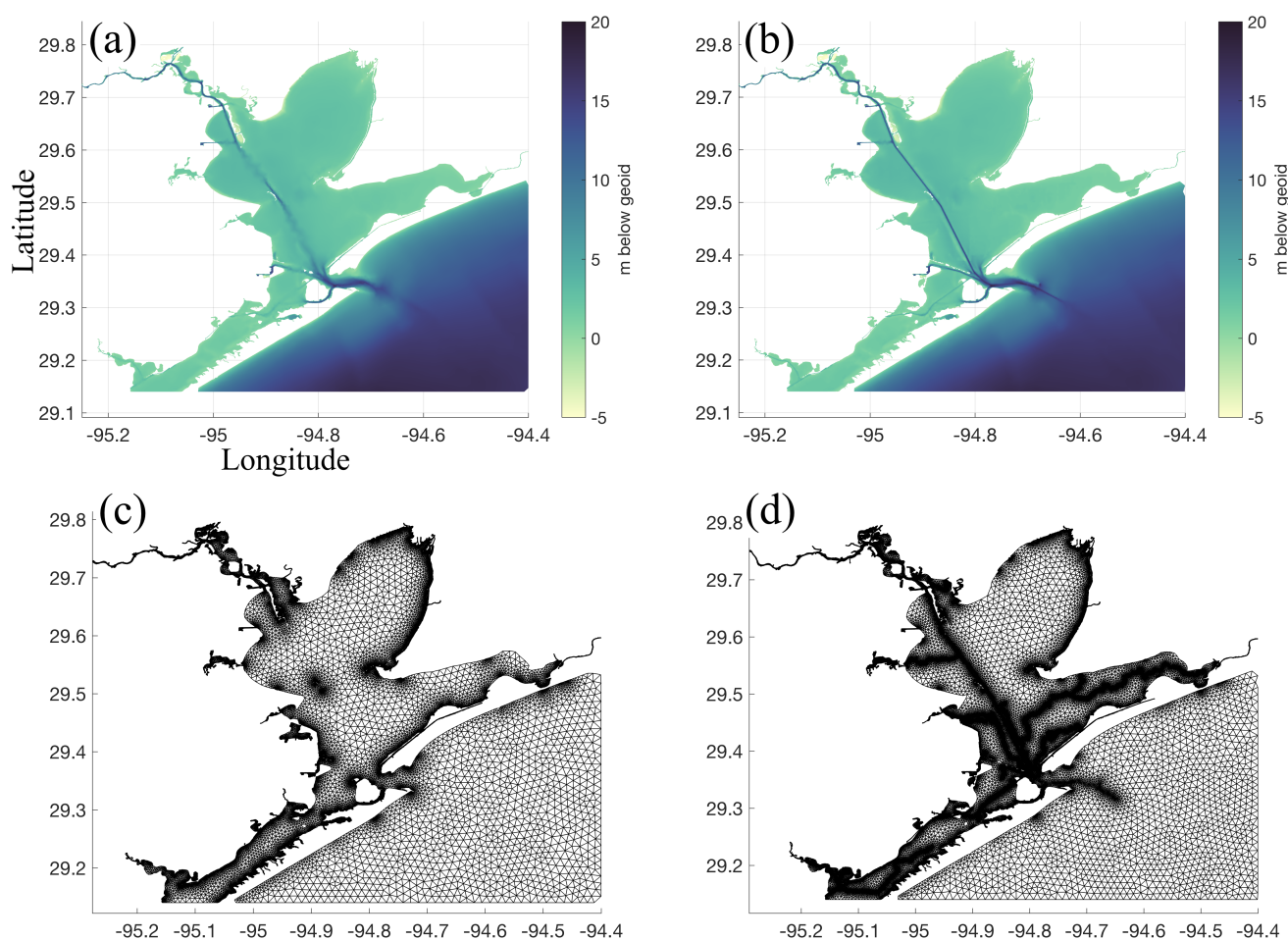
Figure 8. Panels (a) and (c) show the bathymetry and mesh connectivity in the GBAY example (Table 2) created without the thalweg mesh size function enabled; panels (b) and (d) are with the thalweg mesh size function enabled. The 'deep' color palette from cmocean (Thyng et al., 2016) is used in palettes (a) and (b).

Cr as high values tend to give poorer accuracy even in implicit solvers. In a similar approach to Bilgili et al. (2006), for the application of solving the shallow-water equations the Cr can be estimated and bounded in the mesh. We define an estimate of Cr at the vertices of the mesh by adding the shallow water wave speed with an estimate of the anticipated flow speed:

$$Cr = \frac{(u + \sqrt{gH})\Delta t}{\Delta X} \tag{17}$$

5   where u is the magnitude of the flow, g is the acceleration due to gravity, H is the total water depth, Δt is the time step, and ΔX is the element size or the shortest connected edge to each vertex. Since the wave speed is a function of depth and ΔX is equivalent to $h(\boldsymbol{X})$, the user can estimate the CFL condition *a priori* for a given Δt. Note that to obtain this *a priori* estimate of Cr in Eq. (17), we set $H \approx b$, and approximate the flow speed with the long wave linear orbital velocity, i.e., $u \approx \eta\sqrt{g/b}$, where η is the wave amplitude which we set to 1 m by default. Applying these approximations and rearranging gives the

10   following CFL-limiting condition on the edgelength:

$$h(\boldsymbol{X}) \geq \frac{(\eta\sqrt{g/b} + \sqrt{gb})\Delta t}{Cr} \tag{18}$$

where b is set to a minimum of 1 m to allow for the CFL condition to be satisfied overland in the case inundation were to occur.

Thus, the user can specify a value of Δt to bound the mesh resolution based on some value of $Cr < 1$. The aim of CFL-limiting is to help facilitate a mesh to be simulated with a certain time step when using explicit time stepping numerical models.

15   However, this often comes with a loss of mesh resolution that may be critical for resolving important conveyances, so the user must consider reasonable values of Δt based on the minimum edgelength. To avoid this choice, we have also implemented an option (see the User Guide for details on how to invoke) that automatically selects a suitable Δt that satisfies the condition Eq. (18) for the h_{dis} or h_{lfs} (whichever is induced) mesh size functions. The purpose of this is to preserve the nearshore resolution while applying the CFL-limiting to other mesh size functions that may give higher refinement offshore.

20   To demonstrate the CFL-limiting option, we return to the mesh of Jamaica Bay in New York, United States generated using the *feature* mesh size function (Fig. 4). In one rendition of the mesh, no CFL-limiting is used (T_{woCFL}), in another rendition, CFL-limiting with $\Delta t = 2$ s (T_{wCLF}) is invoked. In the generation of T_{wCLF}, the mesh size function is conservatively bounded by $Cr = 0.5$ to allow a buffer for the effects of nonlinearities, bathymetric interpolation, and mesh smoothing. After the mesh is generated, the NCEI Post-Sandy DEM is interpolated onto each vertex using a cell-averaging approach (see *interp* function

25   in User Guide), and the resulting CFL is calculated by Eq. (17) with $\Delta = 2$ s. The use of the CFL-limiter acts to shift the distribution of Cr to smaller values (Fig. 9). The maximum Cr decreases from 3.64 to 0.96 and the mean Cr shifts from 0.68 to 0.36. In the mesh with the CFL-limiting, there are no vertices that violate the CFL condition as compared to 10,492 in the mesh without it. CFL-limiting thus reduces the number of vertices by locally coarsening $h(\boldsymbol{X})$ in fact (T_{wCFL} has 45.6% fewer vertices than T_{woCFL}). Again, the user must be careful when selecting Δt as CFL-limiting may lead to choke points in

30   small channels nearshore which are generally the first areas that violate the CFL (Fig. 10). Depending on the application this may or may not be tolerable.
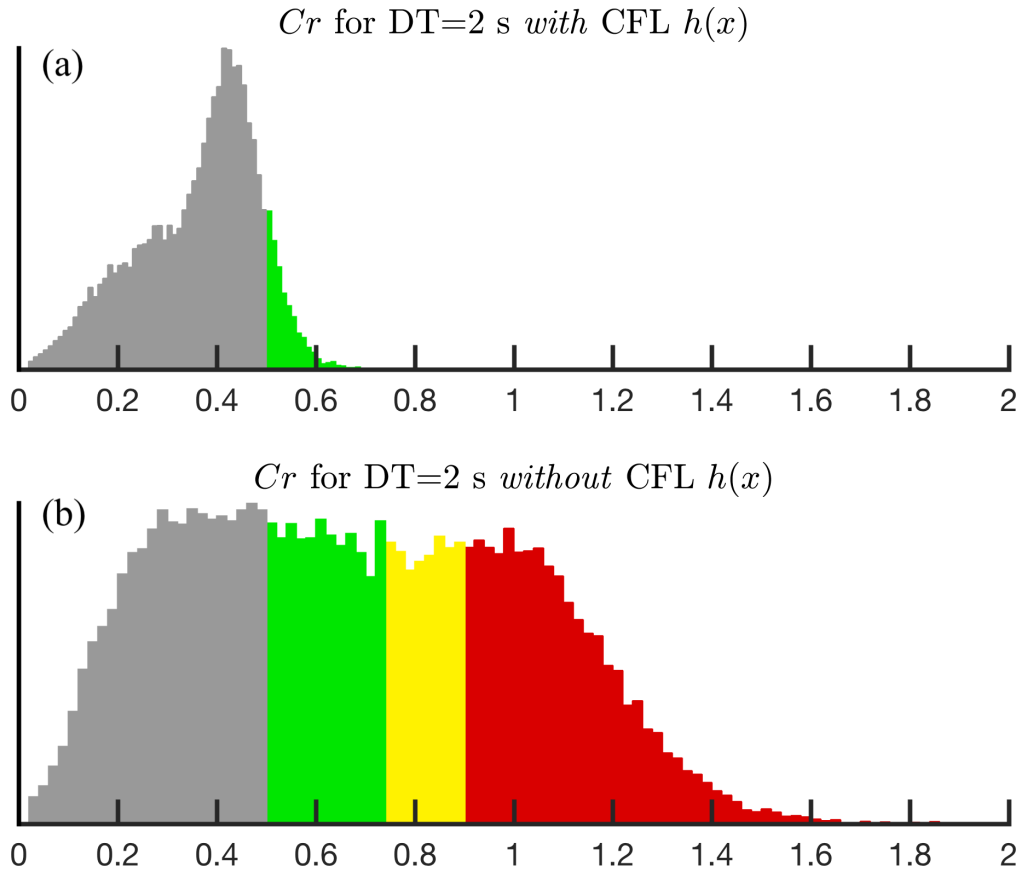
Figure 9. Panel (a) illustrates the effect of CFL-limiting on the Courant number Cr when constructing the JBAY example (Table 2) and (b) without it. The colored bars indicate the vertices with $Cr > 0.5$ and are shown to assist in the comparison of histograms.

Although the above example demonstrates that the Cr of all vertices is reduced to under 1 when using the CFL-limiting mesh size function, the maximum Cr is still 0.96 for a $\Delta t = 2$ s, which may be too close to the theoretical condition to simulate without instabilities. Based on our experience, we need to impose a stricter CFL condition such as $Cr < 0.5$ to ensure numerical stability, accuracy, and minimize numerical artifacts. To ensure that this more conservative condition is fully

5   satisfied, we propose the *CheckTimestep* post-processing function (Algorithm 1). This function iteratively deletes vertices in the mesh associated with edges that violate the CFL. With each deletion, the vertices on the outer fan containing all the connected elements are smoothed using the Laplacian operator. The algorithm relies on MATLAB's implementation of the Bowyer-Watson incremental Delaunay triangulation to preserve the mesh connectivity outside of the modification patch. For example in the JBAY example with CFL-limiting, *CheckTimestep* converged after 5 iterations resulting in a mesh with approximately

10   2,240 less vertices but one that fully satisfied $Cr < 0.5$ everywhere for $\Delta t = 2$ s. In addition to ensuring the CFL condition is fully met, *CheckTimestep* in practice is often used to explore how the mesh would have to be modified in order to achieve a stable simulation for a particular Δt.
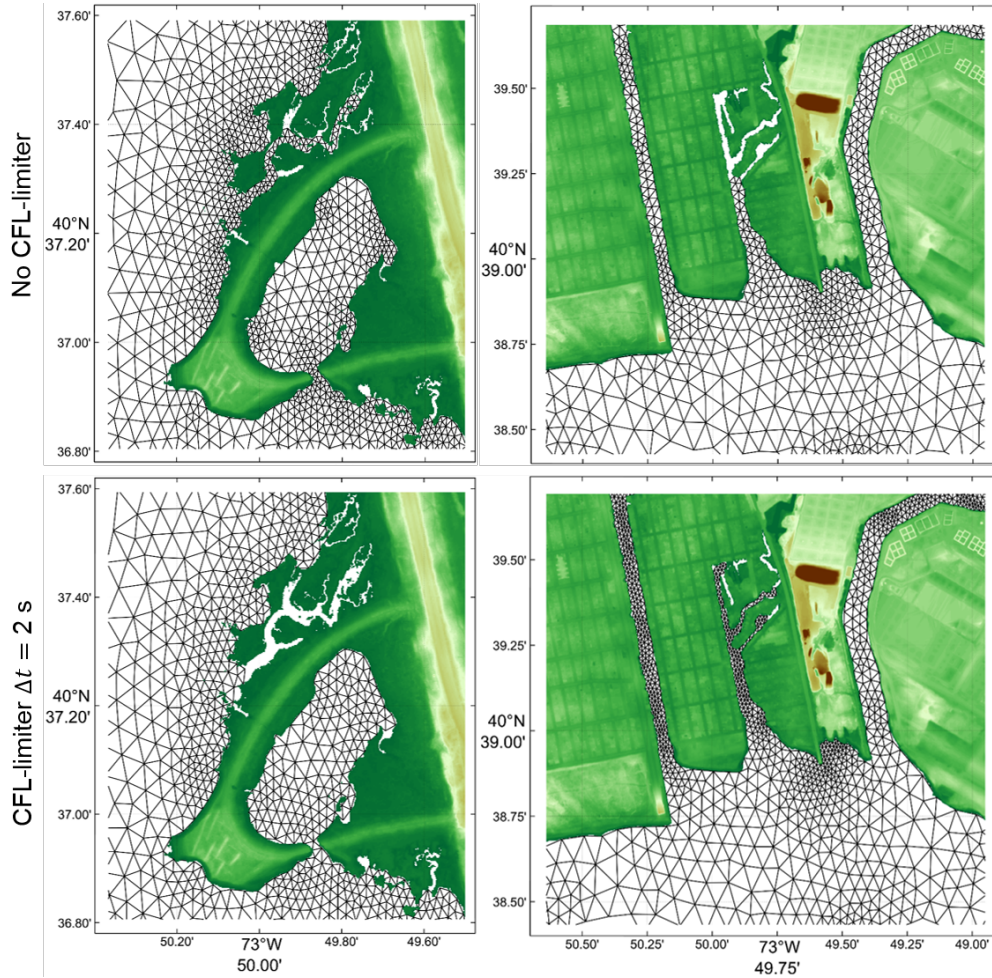
Figure 10. Selected closeup regions in Jamaica Bay, New York (left: West Pond, Queens, right: Old Howard Beach, Queens) of the mesh connectivity built with the JBAY example script. Top panels show the mesh connectivity without invoking the CFL-limiter, and the bottom panels show it when using the CFL-limiting option with $\Delta t = 2$ s.

Algorithm 1 Incrementally adapts a triangulation of points p and connectivity matrix t with bathymetric data b defined at p to a given timestep Δt in seconds through vertex decimation.

1: **Function** $(p,t) = CheckTimestep(p, t, b, \Delta t)$
2: Form nearest neighbor bathymetric interpolant with p, t, and b.
3: Calculate Cr at all vertices using (17) given b, Δt, and the shortest connected edge to the vertex.
4: If $Cr \leq 0.5 \; \forall \; p$, then exit.
5: Otherwise, determine point set p_v with $Cr > 0.5$
6: Incrementally delete p_v from t using Bowyer-Watson algorithm.
7: Apply Laplacian operator to the patch around each p_v containing the connected triangles.
8: Re-interpolate b onto p using nearest-neighbor interpolant and proceed back to 3.

---

5 Mesh generation : *meshgen* class

The purpose of this class is to configure mesh generation related options and subsequently call the mesh generator. The *meshgen* class is a wrapper function around the *DistMesh* algorithm so that it can accept classes that describe Ω and $h(x)$. However, it can be used as a standalone mesh generator.

5 The notion of what constitutes a good quality mesh is application dependent and can be viewed as a combination of geometric element quality measures and application dependencies. For 2D shallow-water flow, a high quality mesh is often determined by geometric quality measures (i.e., nearly all equilateral triangles) with a lower bound on the minimum element quality and the majority of vertices having nearly six edges connected to it (Babuška and Aziz, 1976; Canann et al., 1993; Shewchuk, 2002). When most elements have a high-degree of regularity in the vertex-to-vertex connectivity, it improves the mesh size transitions

10 (grade), the condition number of finite element coefficient matrices, and potentially the memory footprint of the finite element solver (Massey, 2015). A high degree of regularity in the connectivity also tends to coincide with a mesh with many equilateral or nearly equilateral triangles.

5.1 Mesh improvement strategies

The quality of any mesh can be often significantly enhanced through the use of mesh improvement strategies. Approaches

15 for mesh improvement generally can be characterized in three ways: vertex relocation, connectivity adjustments, and addition/deletion of vertices. We present methodologies for both during and after the mesh generation process that combine these three general classes of techniques to improve the final quality of the mesh.

5.1.1 Termination Criterion

Smoothing-based mesh generation approaches, like *DistMesh*, have no theoretical guarantees of minimum triangle quality and

20 thus may take a long time to, or may never, reach a desired quality. The triangle quality (measure of *equilateral-ness*) can be calculated through:

$$q_E = 4\sqrt{3}A_E \left(\sum_{i=1}^{3} (\lambda_E^2)_i \right)^{-1} \tag{19}$$

where A_E is the area of the triangle and $(\lambda_E)_i$ is the length of the ith edge of the triangle. $q_E = 1$ corresponds to an equilateral triangular element and $q_E = 0$ indicates a triangle that degenerates to a line. Persson and Strang (2004) proposed a termination

25 criterion based on convergence to a state where negligible movement of the mesh vertices occurs with additional iterations. In practice, this state is difficult to achieve within a reasonable number of iterations for coastal ocean mesh domains given the fractal shoreline boundary and desired heterogeneous mesh size functions. Thus, we propose an alternative highly-achievable termination criterion based on the distribution of element quality exceeding a triangle-quality threshold:

$$q_{L3\sigma} \equiv \overline{q}_E - 3\sigma_{q_E} > 0.75 \tag{20}$$

where the over-line and σ denote the mean and standard deviation respectively, and $q_{L3\sigma}$ is the "three-sigma lower control limit" element quality, used as a proxy for the minimum element quality. We find that the distribution of the element equality is often Gaussian and that by ensuring Eq. (20) the vast majority (>95%) of the triangles are of adequate quality once this criteria is met. Ideally, we would wish to bound the minimum element quality but, the minimum element quality can be a poor

5 measure of the overall mesh quality for large domains with millions of elements. This is especially the case in our paradigm since a number of mesh cleaning steps are performed *after* this mesh generation termination criterion has been met in order to improve a typically small number of the worst quality triangles.

5.1.2 Strategies during mesh generation

We find that approximately every 10 iterations or so the $q_{L3\sigma}$ element quality starts to saturate. To accelerate convergence,

10 during the mesh generation process the following strategies are conducted every 10 iterations (except item 4 which is executed every iteration):

1. Edges in the mesh that are greater than two times the length as given by $h(\boldsymbol{x}_i)$ (where $\boldsymbol{x}_i$ is the mid point of the edge) are bisected. This creates a new vertex in the center of the bisected edge.

2. Edges that are half as short as their intended length ($h(\boldsymbol{x}_i)$) are deleted.

15 3. A vertex not on the mesh boundary that is connected to less than or equal to four vertices is deleted (this is also performed when the termination criterion is satisfied).

4. Triangles with exceedingly thin angles (< 5°) and large angles (> 175°) are removed every iterations

Improvement strategy one (two) adds (deletes) vertices when they are part of edges that are too long (short), which produces a set of new edges that more closely approximate $h(\boldsymbol{X})$. Improvement strategy three directly reduces the occurrence of small

20 vertex-to-vertex connectivity (valency of three or four), where a valency of six is ideal (Canann et al., 1993). Note that improvement strategy one helps to reduce high vertex-to-vertex connectivity indirectly by avoiding large transitions of element size where larger valencies tend to develop. Improvement strategy four removes flat and obtuse triangles allowing neighboring points to fill these gaps leading to new triangulations that are almost always of better quality.

We demonstrate the benefit from using these mesh improvement strategies through three examples of meshes around the

25 world (Table 2). The time evolution of the geometric element quality demonstrates the benefit directly from these mesh improvement strategies. Figure 11 illustrates that in all three examples the mesh improvement strategies lower the number of iterations necessary to achieve the termination criterion. Further, the rate at which $q_{L3\sigma}$ increases is accelerated in all examples when mesh improvement strategies are enabled. For the development of large multi-scale meshes, 20-50 iterations can often save between 5-20 minutes for the problems here to reach the termination quality.

30 Based on the termination criterion and the improvements listed here, we generally find that complex coastal ocean meshes are generated in approximately 30-100 iterations. Thus, the maximum allowed number of iterations is commonly set to 100, which
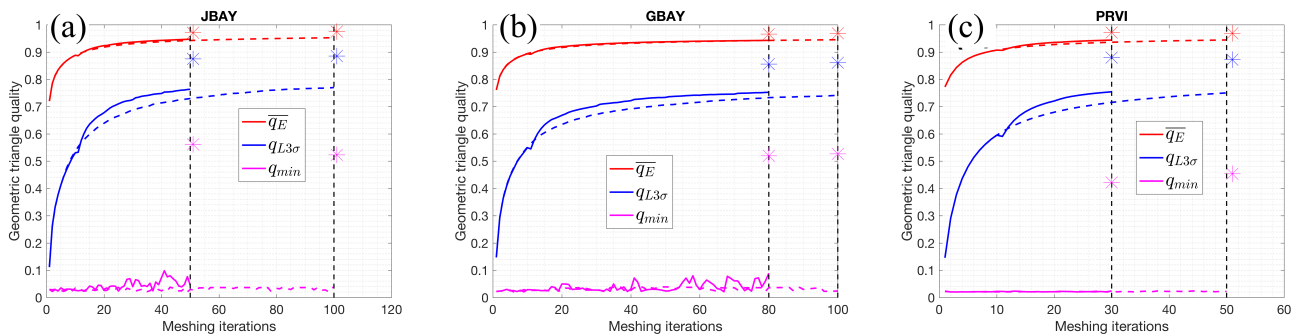
Figure 11. The geometric triangle quality q, Eq. (19), as a function of iterations in the mesh generation process for the three mesh examples (Table 2). The dotted (solid) red (mean), blue (lower third sigma), and magenta (minimum) lines indicate the progression of quality metrics with the mesh improvement strategies turned off (on) during mesh generation. At the end of mesh generation, a secondary round of mesh improvement strategies are applied and the resulting quality after this step is indicated by the colored asterisk. In each panel, the dotted vertical black line demarcates when the mesh generation process finished.

typically takes a few minutes to half an hour to compute depending primarily on the boundary manifoldness and minimum element size.

5.1.3 Strategies after mesh generation

After mesh generation has terminated, we apply a secondary round of mesh improvement strategies focused towards improving
5 the geometrically worst quality triangles, which often occur near the boundary of the mesh and can make simulation impossible. Poor quality triangles typically occur near the mesh boundary because narrow channels and restricted connections between bodies of water may be difficult or impossible to resolve given the user requested minimum mesh resolution. Since we did not rely on a shoreline simplification strategy to avoid incongruities between the underlying geophysical data and the minimum mesh size, we instead employ a handful of algorithms that exhaustively address problems that typically arise. The end result is
10 a simplified mesh boundary that conforms well to the user-requested minimum element size and can be simulated.

In order to simulate with a given mesh, it is essential to that there are no topological defects that make simulation impossible. We call a mesh with none of the following defects valid. A valid mesh in our work is defined by having the following properties:

1. The vertices of each triangle are arranged in the counter-clockwise order.

2. There mesh is conformal: a triangle is not allowed to have a vertex of another triangle in its interior.

15 3. The boundary of the mesh can only be traversed from any starting point on it by only visiting *unique* boundary points that are connected together by an segment.

Properties one and two are handled with the *fixmesh.m* function that was provided with the original *DistMesh* package. Property three is often not satisfied upon termination of the mesh generator because a simplification of the shoreline was not applied. Fragmented patches of triangles result near the shoreline boundary and can destroy the uniqueness of the mesh's boundary

path, which we call traversability. Note that property three can be more simply expressed as requiring the number of boundary segments to be equal to the number of boundary vertices.

Algorithm 2 Given a triangulation composed of vertices p and triangle connectivity matrix t return a p and t that has only two traversal paths along its boundaries in which disjoint portions of the mesh that each make up less than a specified area-fraction μ_{co} of the initial total mesh area (or less than a specified absolute area in km^2 when $\mu_{co} \geq 1$), have been removed

Function $(p,t) = Make\_Mesh\_Boundaries\_Traversable(p, t, \mu_{co})$
Get mesh boundary edges and vertices
while number of boundary edges > number of boundary vertices **do**
  call Delete_Exterior_Elements(t,μ_{co})
  Delete non-conformal vertices and renumber
  call Delete_Interior_Elements(p,t)
  Delete non-conformal vertices and renumber
  Get mesh boundary edges and vertices
end while

Function $t = Delete\_Exterior\_Elements(t, \mu_{co})$
$A \leftarrow$ area of t [km^2]
$t_1 \leftarrow t$, and $t \leftarrow \emptyset$
$A_1 \leftarrow$ area of t_1 [km^2]
while ($A_1/A > \mu_{co}$ when $\mu_{co} < 1$) *or* ($A_1 > \mu_{co}$ when $\mu_{co} \geq 1$) **do**
  Get the element adjacency table
  $s \leftarrow$ random element in t_1
  Beginning at s, perform a breadth-first search (BFS) of t_1 to get a connected subset of
  elements, t_2
  $A_2 \leftarrow$ area of t_2 [km^2]
  if ($A_2/A > \mu_{co}$ when $\mu_{co} < 1$) *or* ($A_2 > \mu_{co}$ when $\mu_{co} \geq 1$) **then**
    Keep t_2 by adding it onto t
  end if
  Delete t_2 from t_1
  $A_1 \leftarrow$ new area of t_1 [km^2]
end while

Function $t = Delete\_Interior\_Elements(p, t)$
Get mesh boundary edges
$bad \leftarrow$ boundary vertices that have more than two connecting boundary edges
Get the vertex to element adjacency table
for each i in bad **do**
  $t_1 \leftarrow$ elements connected to vertex i that have two boundary edges
  $L_1 \leftarrow$ number of elements in t_1
  if $L_1 == 1$ **then**
    Delete t_1 from t
  else if $L_1 > 1$ **then**
    Delete the worst quality element in t_1 from t
  else
    Delete the worst quality element connected to vertex i from t
  end if
end for

A *Make_Mesh_Boundaries_traversable* function (Algorithm 2) was developed to remove fragmented patches of elements that are either disconnected from the major portion of the mesh (that may or may not affect the mesh boundary traversability),

or are not-disconnected but are responsible for destroying the mesh boundary traversability. The former set of fragmented elements are defined as being "exterior" disjoint components of the mesh where, starting from a random seed element in the mesh, the total area of a connected set of elements (i.e., elements that share an edge) is smaller than a user-defined threshold μ_{co}, which is defined in terms of either the total mesh area-fraction or an absolute area cutoff (by default we set $\mu_{co} = 0.25$ which is

5   equivalent to a 25% total mesh area-fraction cutoff). These patches are identified and deleted by the *Delete_Exterior_Elements* sub-function (Algorithm 2) through the use of a breadth-first search (BFS). The latter set of fragmented elements are defined as being "interior" elements of the mesh that interfere with the traversability of the mesh boundary path that are not caught by the *Delete_Exterior_Elements* sub-function. The *Delete_Interior_Elements* sub-function (Algorithm 2) deals with identifying and deleting these elements. In this sub-function, an offending vertex is first identified that has more than two connecting boundary

10   edges. One of the elements connected to this vertex is chosen to be deleted based on, first, triangles that have two boundary edges, and second, triangles with the lowest quality, q_E. Further details of *Make_Mesh_Boundaries_traversable* and examples of the elements that it deletes is included in the User Guide.

After the mesh's boundary is made traversable, boundary triangles that are connected to just a single neighboring triangle are removed exhaustively by the *Fix_single_connec_edge_elements* sub-function. The singly-connected triangles are removed be-

15   cause they are not well-constrained during mesh generation and often poorly represent the shoreline geometry and bathymetry. Further, singly-connected triangles can artificially constrict the exchange of water through narrow water courses when logic-based wetting/drying algorithms are used.

While non-boundary vertices connected to four or less vertices are deleted during the mesh generation process and on termination, vertices with high vertex-to-vertex connectivity are not directly dealt with in the generation process. However, we

20   do find that the periodic splitting of long edges (compared to $h(x)$) and the smoothing of the mesh size function ensures that almost all of the vertices in the mesh have good vertex-to-vertex connectivity (i.e., close to six) with a typical upper bound of eight. Although connectivity higher than eight is less common, the *bound_con_int* function that was described and originally coded by Massey (2015) is used after the *Fix_single_connec_edge_elements* function to bound the vertex-to-vertex connectivity in the entire mesh to eight. It is possible to use the *bound_con_int* function to bound the vertex-to-vertex connectivity to seven,

25   but convergence may take a considerable amount of time so this is excluded from the standard procedure. Instead, the user may invoke the *bound_con_int* function as an additional procedure in an attempt to bound the vertex-to-vertex connectivity to seven.

The final function that is applied to the mesh in the cleaning process is *direct_smoother_lur*, which provides additional smoothing to the non-boundary vertices through a single-step implicit operation (Balendran, 1999). Applying this function can

30   often dramatically enhance the statistical distribution of q_E. This can be seen in the time series of the geometric element quality where upon execution of the clean-up routine, the minimum triangle quality improves from <5% to 40-60% (Fig. 11). One drawback is that the implicit smoother does not take into account the mesh size distribution. Thus, it is important to ensure that enough iterations of the *DistMesh* algorithm have been conducted so that the triangles are mostly of high quality and conform well to the $h(\boldsymbol{X})$ before applying *direct_smoother_lur*. Note that for best results using *direct_smoother_lur*, elongated mesh
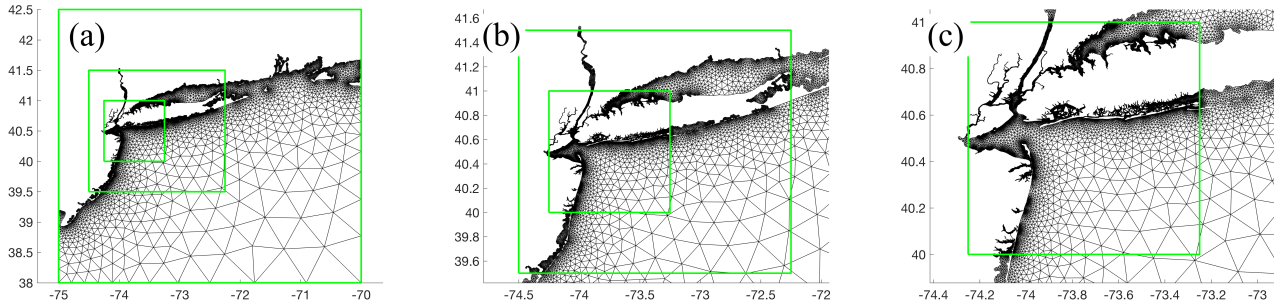
Figure 12. An example of the multiscale meshing technique applied to a set of domains around the New York/Long Island area. The green boxes are specified by the user. The minimum resolution of the outermost green box in each panel is different: (a) it is 1 km, (b) 500 m, and (c) 35 m. Notice how the regions of overlap gradually transition into each other.

boundary elements that have poor element quality (we choose $q_E < 0.5$) are deleted before beginning the post-processing mesh improvement steps.

5.2 Support for multiple *edgefx* and *geodata* inputs (multiscale meshing approach)

The geospatial data used to generate mesh size functions often have varying horizontal resolutions and non-overlapping cov-
5 erage interspersed with large areas where only coarser global datasets are available. Typically, users want to mesh localized regions down to the estuarine-scale with comparatively finer resolution (where high quality geospatial datasets are available) and use coarser resolution elsewhere. In these situations, the Cartesian mesh size function approach employed (Sect. 4) is largely memory and computationally inefficient since it requires a uniform minimum spacing to form the mesh size function and to conduct the initial point rejection in the *DistMesh* algorithm. More fundamentally, for shallow water flow it is unneces-
10 sary to use fine mesh resolution in deeper waters because the dominant length scale grows according to the Rossby radius of deformation to thousands of kilometers (LeBlond, 1991).

To address this issue, the *meshgen* class has been developed to allow the user to pass multiple instances of the boundary description (*geodata*) and mesh size (*edgefx*) classes to the *meshgen* class, an approach that we term 'multiscale meshing'. Instances of these classes are defined within axis-aligned bounding boxes (rectangles) that can be partially or fully nested any
15 number of times with largely disparate mesh sizes between nests (Fig. 12).

The major requirement when using this approach is that the instances must be provided in order of *decreasing* minimum mesh size (i.e., coarse ⇒ fine). Note that overlapping regions of the same minimum mesh size are also allowed. An additional requirement is that the coarsest (largest) instance of these classes, which acts as the absolute mesh boundary, must completely encompass all finer instances in space. A key computational benefit of this multiscale meshing approach is that it still enjoys
20 the simplicity and speed associated with structured mesh size function grids as we mentioned in Sect. 4 but offers the user more control over how the available geospatial data is used in the mesh generation process.

Table 4. Wall-clock time in seconds (% of total) for the steps involved in mesh generation. The pre-processing includes reading and processing the geospatial data (in *geodata*) and forming the mesh size functions (in *edgefx*). The vertex relocation timings include the time elapsed in the initial point rejection, vertex re-projection back into Ω, vertex movement, and mesh improvement strategies (in *meshgen.build*). The cleaning category includes the time spent in the methods documented in Sect. 5.1.3 (*meshgen.clean*).

Example	Pre-processing time	Mesh generation time			Total Time
		Vertex relocation	**Triangulation**	**Cleaning**	
JBAY	13.7 (22.5%)	24.9 (41.0%)	18.3 (30.0%)	3.83 (6.25%)	60.8
GBAY	23.9 (25.1%)	34.1 (35.8%)	31.4 (33.0%)	5.79 (6.09%)	95.2
PRVI	1,770 (64.1%)	498 (18.1%)	316 (11.5%)	174 (6.31%)	2,760

The OOP framework (Sect. 2) is integral to enabling this approach because multiple instances of the *geodata* and *edgefx* classes can be generated independently from each other. Thus, only minor modifications and additions to the *meshgen* class were required to facilitate the approach. An important additional routine (*smooth_outer.m* that is called during the execution of *meshgen()* when multiple *edgefx* classes are present was developed to ensure a smooth transition between instances of disparate

5 mesh resolution by using the marching method (*limgradStruct.m*, Persson, 2006). The mesh size function of an *edgefx* instance is updated in areas of overlap using the mesh size function of comparatively higher resolution. The mesh size function of the coarser *edgefx* instance that was updated is subsequently smoothed using the *limgradStruct.m* function.

This approach is similar to the multi-grid nesting technique employed by ocean models (e.g. Debreu et al., 2012; Brown et al., 2016; Pringle et al., 2018) but in the finite element framework without the need for a coupling paradigm. The application of this

10 method allows for the construction of a seamless unstructured mesh with edgelength transitions bounded by the user-defined allowable limit α_g to be generated, but does not alter resolution significantly in the insets away from the boundaries of their bounding boxes. This makes our approach particularly beneficial over traditional structured multi-grid nesting approaches employed by ocean models because it avoids issues associated with interpolation and smoothing at the interfaces between disparate resolution grids that ultimately reduce numerical accuracy.

15 Figure 13 illustrates an example of using multiple *edgefx* and *geodata* instances to construct a locally high resolution mesh (minimum resolution of 10-30 m) around Puerto Rico and the U.S. Virgin Islands (PRVI), embedded within a significantly larger western North Atlantic mesh domain (minimum resolution of 1 km); see Table 2. The resulting seamless mesh is generated from one global DEM (SRTM15_PLUS, 30 arc-second resolution) and three local DEMs. Two of the local DEMs have 1 arc-second resolution and cover the general PRVI region. The other local DEM covers a small region around San Juan, Puerto

20 Rico with 1/9 arc-second resolution. High resolution coastlines are extracted from the local DEMs using the r.contour module in GRASS GIS. Note how the mesh seamlessly transitions between the extents of DEMs that are used to create each local *geodata* and *edgefx* class (Fig. 13).
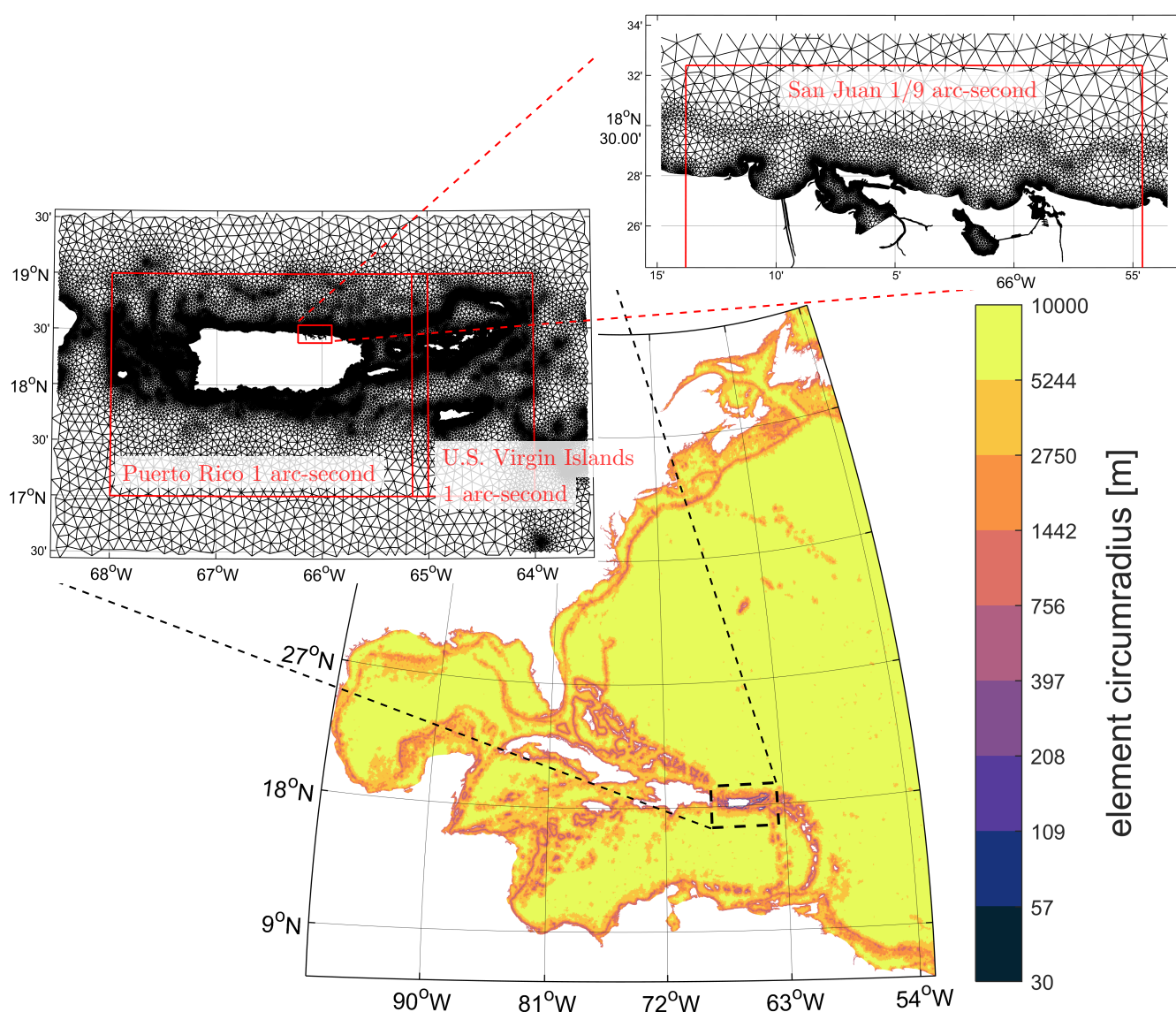
Figure 13. PRVI example (see Table 2) that uses a multiscale meshing approach to produce a seamless unstructured mesh with locally high mesh resolution insets. Regional DEMs (names and extents annotated on figure) are used to mesh in high resolution around Puerto Rico and the U.S Virgin Islands ($h0 = 30$ m), including very high resolution around San Juan ($h0 = 10$ m). These are nested within a mesh covering the entire western North Atlantic Ocean built using global SRTM15_PLUS bathymetry ($h0 = 1$ km), in which the local mesh resolution is shown here.

6 Mesh Generation Wall-Clock Time

The total and component-based wall-clock times for generating each of the three examples presented in this study is shown in Table 4. Overall, the small examples (JBAY and GBAY) complete in under 2 minutes, and the large PRVI example takes approximately 45 minutes. Consistently for all examples vertex relocation consumes slightly more time than Delaunay triangulation, and the mesh cleaning (post-processing improvement strategies) accounts for approximately 6% of the total time. The relative balance between mesh generation and pre-processing times depends on the resolution of the shoreline and the size of the meshing domain. For example, in the small domain problems (JBAY and GBAY), the pre-processing time makes up roughly a quarter of the total time. In contrast, in the PRVI example which meshes most of the north western Atlantic ocean using four separate *geodata* and *edgefx* classes, the pre-processing time accounts for 64% of the total time. Therefore, while it is likely possible to speed-up the mesh generation process through e.g., parallel Deluanay triangulation and/or different approaches to the initial point rejection in the *DistMesh* algorithm, for large and complex meshes intelligent use of the multiscale meshing approach combined with parallelization of the construction of the individual *edgefx* and *geodata* classes is likely to result in the greatest speedup.

7 Discussion and conclusions

A toolkit to create unstructured meshes composed of two-dimensional (2D) triangular elements for coastal ocean models was developed by modifying the *DistMesh* algorithm for the type of geophysical domains encountered in coastal ocean problems. This software was embedded into an object-orientated approach composed of four standalone MATLAB classes that complement each other to simplify the necessary pre- and post- processing procedures for mesh generation. The overarching goal of these tools is to reduce the complexity and hours spent constructing real-world meshes to the degree that it allows one to more carefully and systemically study the impact on the coastal circulation attributed to mesh refinement.

A set of common coastal ocean relevant mesh size functions were built into the mesh size function class (*edgefx*) that can handle a variety of user-based constraints and ensure the mesh connectivity can be reproduced on a personal computer. The implementation of these mesh size functions were largely borrowed from pre-existing literature with some minor enhancements. We presented a polyline mesh size function to locally enhance resolution around and near marine navigation channels and deep-draft channels (i.e. thalwegs). These features were found by thresholding upslope-area calculated from a digital elevation model (DEM) using GIS software. The polyline mesh size function may have interesting future applications for the development of overland meshes that seamlessly mate with ocean meshes. For example, the user could provide a set of lines that characterize overland ridges so that the polyline mesh size function can be used to locally enhance mesh resolution to better capture the local maximums in the topographic heights. Since the representation of the inter-tidal and floodplain zone in the mesh is critical for coastal flooding applications, ensuring overland features like hills and levees are correctly represented in the mesh is a important feature. In its current state, the toolbox is able to constrain piecewise linear segments that may represent e.g., a series of levees; however, if there is a large degree of disparity between the point spacing on the constraints and the mesh size function, then the resulting mesh will be of poor quality.

To ensure that a mesh would be computationally stable with a user-requested time step (relevant when simulating with explicit/semi-implicit numerical models), a CFL-limiting mesh size function similar to (Bilgili et al., 2006) was introduced. In this approach, we estimate the Courant (Cr) number based on shallow water wave theory and ensure that the final mesh size function satisfies the CFL condition ($Cr < 1$). Although applying CFL-limiting to the mesh size function was shown to

5   help encourage stability by lowering the Cr, the resulting unstructured mesh may not necessarily satisfy the CFL condition due to that fact that bathymetric interpolation from the DEM is not easily constrained. Thus, an iterative algorithm to be applied *after* the mesh was developed (*CheckTimestep*) to locally alter the connectivity by decimating vertices that violate the CFL condition. Depending on the users choice of time step and the various mesh size constraints, the algorithm decimates vertices in certain regions (e.g, small constricted channels) that may or may not be tolerable for the problem at hand. In such

10   regions, anisotropic mesh elements (e.g. Piggott et al., 2009) that could be generated using mesh size functions which include a directional component may be more beneficial than isotropic equilateral elements. Thus, implementing anisotropic mesh size functions into the software, along with the testing of the resultant meshes in real coastal ocean problems, is an interesting direction for future work.

We emphasized the expensive nature of building large-scale high-fidelity mesh size functions which motivates the use of

15   a multiscale meshing approach. This approach reflects the often sparse spatial coverage and heterogeneous nature of freely available digital elevation data that are often used in the construction of the mesh size functions. Multiscale meshing allows the user to build (extremely) high resolution local mesh size functions that are embedded in larger scale ocean domains. The end result is a mesh that seamlessly transitions from the high refinement region to coarser elements outside the region of interest. This is practically useful to accurately model coastal flooding in small regions (e.g., a city or a small island – here we show

20   an example of the approach with the mesh refinement region around Puerto Rico and the U.S. Virgin Islands) that may be susceptible to storms and tropical cyclones (TC) passing over it. For large-scale TC-driven storm surge events, it has been shown that a large model domain is essential to capture the pre-event conditions that can alter the modeled severity of the event (Blain et al., 1994). In forecasting scenarios, the multiscale meshing approach could be used to mesh around the predicted land-falling region based on the cone of uncertainty of the path of the storm to locally higher resolution. This approach could

25   generate meshes for the prediction of coastal flooding on-the-fly as new forecast data becomes available. Given the local nature of the mesh refinement in this approach, these meshes could be computationally more efficient with smaller minimum element sizes than pre-existing ones, (e.g., the U.S. National Ocean Service's (NOS) Hurricane Storm Surge Operational Forecast System (HSSOFS) mesh, Technology Riverside Inc. and AECOM, 2015), which cover entire swaths of coastline with medium level resolution.

30   Three examples were used for demonstration in this study (Table 2). A further three separate examples are illustrated in the User Guide (Roberts and Pringle, 2018). All six examples are released with this version of the OceanMesh2D package. They can be used to become familiar with the software, for testing purposes, and as templates for scripts used to generate the user's custom mesh.

Code availability. The OceanMesh2D mesh generator toolbox is hosted on the following GitHub page: https://github.com/CHLNDDEV/ OceanMesh2D. The version release presented in this paper is available as a Zenodo archive: https://doi.org/10.5281/zenodo.1341385. The software requires no paid MATLAB toolboxes to generate meshes; however, some auxiliary functions (e.g., those that create ADCIRC input files) not used in primary workflows may. A User Guide (Roberts and Pringle, 2018) and a suite of examples is available from the main
5 GitHub page. All components of the OceanMesh2D toolbox are free software, being released under the GNU General Public License version 3.0. Full details of the license, including the compatible copyright notices of third party routines included in the package, are provided in the LICENSE file in the source distribution.

Author contributions. KR designed the framework of the software. KR and WP equally contributed to the coding and development of the software, design and testing of the provided examples, and the preparation of the manuscript and its associated figures. JW provided the
10 research environment and intellectual discussion necessary for the software's development and eventual realization of this manuscript.

Competing interests. The authors declare that they have no conflict of interest.

Acknowledgements. We thank Dr. Darren Engwirda at Columbia University in the City of New York for the useful functions that are available through the MathWorks website. Our gratitudes to Dr. Chris Massey at US Army Corps of Engineers ERDC Coastal and Hydraulics Laboratory for his function to bound the vertex connectivity. The m_map (https://www.eoas.ubc.ca/~rich/map.html) and cmocean (Thyng
15 et al., 2016) (https://matplotlib.org/cmocean/) toolboxes are widely used in plotting and mapping related routines within OceanMesh2D, for which we are grateful for the authors' work. We appreciate the valuable feedback provided by Dr. Darren Engwirda and Professor Per-Olof Persson at the University of California, Berkeley. The authors wish to thank Dr. Damrongsak Wirasaet at the University of Notre Dame for many helpful discussions and his comments on an initial draft that lead to an improvement in the quality of this manuscript. This work was supported in part by the National Science Foundation under grant ACI-1339738.

References

Arya, S. and Mount, D. M.: Approximate Nearest Neighbor Queries in Fixed Dimensions, in: Proc. 4th Ann. ACM-SIAM Symposium on Discrete Algorithms (SODA), pp. 271–280, 1993.

Babuška, I. and Aziz, A.: On the Angle Condition in the Finite Element Method, SIAM Journal on Numerical Analysis, 13, 214–226, https://doi.org/10.1137/0713021, 1976.

Bagon, S.: Matlab class for ANN, available at http://www.wisdom.weizmann.ac.il/~bagon/matlab.html, 2009.

Balendran, B.: A Direct Smoothing Method for Surface Meshes, in: Proceedings of the 8th International Meshing Roundtable, South Lake Tahoe, California, USA, October 10-13, 1999, pp. 189–193, http://imr.sandia.gov/papers/abstracts/Ba142.html, 1999.

Becker, J. J., Sandwell, D. T., Smith, W. H. F., Braud, J., Binder, B., Depner, J., Fabre, D., Factor, J., Ingalls, S., Kim, S.-H., Ladner, R., Marks, K., Nelson, S., Pharaoh, A., Trimmer, R., Von Rosenberg, J., Wallace, G., and Weatherall, P.: Global Bathymetry and Elevation Data at 30 Arc Seconds Resolution: SRTM30_PLUS, Marine Geodesy, 32, 355–371, https://doi.org/10.1080/01490410903297766, 2009.

Bilgili, A., Smith, K. W., and Lynch, D. R.: BatTri: A two-dimensional bathymetry-based unstructured triangular grid generator for finite element circulation modeling, Computers and Geosciences, 32, 632 – 642, https://doi.org/10.1016/j.cageo.2005.09.007, 2006.

Blain, C. A., Westerink, J. J., and Luettich R A., .: The influence of domain size on the response characteristics of a hurricane storm surge model, Journal of Geophysical Research, 99, 467–479, https://doi.org/10.1029/94JC01348, 1994.

Brown, J. M., Norman, D. L., Amoudry, L. O., and Souza, A. J.: Impact of operational model nesting approaches and inherent errors for coastal simulations, Ocean Modelling, 107, 48–63, https://doi.org/10.1016/j.ocemod.2016.10.005, 2016.

Brufau, P., Garcã, P., and Vã, M. E.: Zero mass error using unsteady wetting–drying conditions in shallow flows over dry irregular topography, International Journal for Numerical Methods in Fluids, 1082, 1047–1082, https://doi.org/10.1002/fld.729, 2004.

Canann, S. A., Stephenson, M. B., and Blacker, T.: Optismoothing: An optimization-driven approach to mesh smoothing, Finite Elements in Analysis and Design, 13, 185 – 190, https://doi.org/10.1016/0168-874X(93)90056-V, 1993.

Candy, A. and Pietrzak, J.: Shingle 2.0: Generalising self-consistent and automated domain discretisation for multi-scale geophysical models, Geoscientific Model Development, pp. 213–234, https://doi.org/10.5194/gmd-11-213-2018, 2018.

Candy, A. S., Avdis, A., Hill, J., Gorman, G. J., and Piggott, M. D.: Integration of Geographic Information System frameworks into domain discretisation and meshing processes for geophysical models, Geoscientific Model Development Discussions, 7, 5993–6060, https://doi.org/10.5194/gmdd-7-5993-2014, 2014.

Conroy, C. J., Kubatko, E. J., and West, D. W.: ADMESH:An advanced, automatic unstructured mesh generator for shallow water models, Ocean Dynamics, 62, 1503–1517, https://doi.org/10.1007/s10236-012-0574-0, 2012.

Debreu, L., Marchesiello, P., Penven, P., and Cambon, G.: Two-way nesting in split-explicit ocean models: Algorithms, implementation and validation, Ocean Modelling, 49-50, 1–21, https://doi.org/10.1016/j.ocemod.2012.03.003, 2012.

Eakins, B. W. and Taylor, L.: Seamlessly integrating bathymetric and topographic data to support tsunami modeling and forecasting efforts, in: Ocean Globe, edited by Breman, J., chap. 2, pp. 37–56, ESRI Press, https://www.ngdc.noaa.gov/mgg/coastal/OceanGlobe_chapter2.pdf, 2010.

Eakins, B. W., Danielson, J. J., Sutherland, M. G., and Mclean, S. J.: A framework for a seamless depiction of merged bathymetry and topography along U.S. coasts, in: Proc. of U.S. HYDRO, p. 10, National Harbor, MD, https://www.ngdc.noaa.gov/mgg/inundation/sandy/data/doc/Topobathy_DEM_framework.pdf, 2015.

Engsig-Karup, A. P., Hesthaven, J. S., Bingham, H. B., and Warburton, T.: DG-FEM solution for nonlinear wave-structure interaction using Boussinesq-type equations, Coastal Engineering, 55, 197 – 208, https://doi.org/10.1016/j.coastaleng.2007.09.005, 2008.

Engwirda, D.: Locally optimal Delaunay-refinement and optimisation-based mesh generation, Ph.D. thesis, University of Sydney, http://hdl.handle.net/2123/13148, 2014.

5   Engwirda, D.: JIGSAW-GEO (1.0): Locally orthogonal staggered unstructured grid generation for general circulation modelling on the sphere, Geoscientific Model Development, 10, 2117–2140, https://doi.org/10.5194/gmd-10-2117-2017, 2017.

Gorman, G., Piggott, M., Pain, C., de Oliveira, C., Umpleby, A., and Goddard, A.: Optimisation based bathymetry approximation through constrained unstructured mesh adaptivity, Ocean Modelling, 12, 436 – 452, https://doi.org/10.1016/j.ocemod.2005.09.004, 2006.

Gorman, G., Piggott, M., Wells, M., Pain, C., and Allison, P.: A systematic approach to unstructured mesh generation for ocean modelling
10   using GMT and Terreno, Computers and Geosciences, 34, 1721–1731, https://doi.org/10.1016/j.cageo.2007.06.014, 2008.

GRASS Development Team: Geographic Resources Analysis Support System (GRASS GIS) Software, Version 7.2, Open Source Geospatial Foundation, http://grass.osgeo.org, 2017.

Greenberg, D. A., Dupont, F., Lyard, F. H., Lynch, D. R., and Werner, F. E.: Resolution issues in numerical models of oceanic and coastal circulation, Continental Shelf Research, 27, 1317 – 1343, https://doi.org/10.1016/j.csr.2007.01.023, recent Developments in Physical
15   Oceanographic Modelling: Part IV, 2007.

Hagen, S. C., Horstmann, O., and Bennett, R. J.: An Unstructured Mesh Generation Algorithm for Shallow Water Modeling, International Journal of Computational Fluid Dynamics, 16, 83–91, https://doi.org/10.1080/10618560290017176, 2002.

Heinzer, T. J., Williams, M. D., Dogrul, E. C., Kadir, T. N., Brush, C. F., and Chung, F. I.: Implementation of a feature-constraint mesh generation algorithm within a GIS, Computers and Geosciences, 49, 46 – 52, https://doi.org/10.1016/j.cageo.2012.06.004, 2012.

20   Huthnance, J. M.: Circulation, exchange and water masses at the ocean margin: the role of physical processes at the shelf edge, Progress in Oceanography, 35, 353 – 431, https://doi.org/10.1016/0079-6611(95)80003-C, 1995.

Koko, J.: A Matlab mesh generator for the two-dimensional finite element method, Applied Mathematics and Computation, 250, 650–664, https://doi.org/10.1016/j.amc.2014.11.009, 2015.

Lambrechts, J., Comblen, R., Legat, V., Geuzaine, C., and Remacle, J.-F.: Multiscale mesh generation on the sphere, Ocean Dynamics, 58,
25   461–473, https://doi.org/10.1007/s10236-008-0148-3, 2008.

Le Provost, C. and Lyard, F.: Energetics of the M2 barotropic ocean tides: an estimate of bottom friction dissipation from a hydrodynamic model, Progress in Oceanography, 40, 37–52, https://doi.org/10.1016/S0079-6611(97)00022-0, 1997.

LeBlond, P. H.: Tides and their Interactions with Other Oceanographic Phenomena in Shallow Water (Review), in: Tidal hydrodynamics, edited by Parker, B. B., pp. 357–378, John Wiley & Sons, Inc., New York, USA, 1991.

30   Liu, J.: Open and traction boundary conditions for the incompressible Navier–Stokes equations, Journal of Computational Physics, 228, 7250 – 7267, https://doi.org/10.1016/j.jcp.2009.06.021, 2009.

Luettich, R. and Westerink, J. J.: Formulation and Numerical Implementation of the 2D/3D ADCIRC Finite Element Model Version 44.XX, Tech. rep., http://www.unc.edu/ims/adcirc/adcirc_theory_2004_12_08.pdf, 2004.

Luettich, R. A. and Westerink, J. J.: Continental Shelf Scale Convergence Studies with a Barotropic Tidal Model, chap. 16, pp. 349–371,
35   American Geophysical Union (AGU), https://doi.org/10.1029/CE047p0349, 2013.

Lyard, F., Lefevre, F., Letellier, T., and Francis, O.: Modelling the global ocean tides: modern insights from FES2004, Ocean Dynamics, 56, 394–415, https://doi.org/10.1007/s10236-006-0086-x, 2006.

Massey, T. C.: Locally constrained nodal connectivity refinement procedures for unstructured triangular finite element meshes, Engineering with Computers, 31, 375–386, https://doi.org/10.1007/s00366-014-0357-y, 2015.

Mount, D. M. and Arya, S.: ANN: A Library for Approximate Nearest Neighbor Searching, version 1.1.1, available at http://www.cs.umd.edu/~mount/ANN/, 2006.

5 Nguyen, V.-T., Peraire, J., Khoo, B. C., and Persson, P.-O.: A discontinuous Galerkin front tracking method for two-phase flows with surface tension, Computers & Fluids, 39, 1 – 14, https://doi.org/10.1016/j.compfluid.2009.06.007, 2010.

O'Callaghan, J. F. and Mark, D. M.: The extraction of drainage networks from digital elevation data, Computer Vision, Graphics, and Image Processing, 28, 323 – 344, https://doi.org/10.1016/S0734-189X(84)80011-0, 1984.

Persson, P. O.: Mesh size functions for implicit geometries and PDE-based gradient limiting, Engineering with Computers, 22, 95–109,
10 https://doi.org/10.1007/s00366-006-0014-1, 2006.

Persson, P. O. and Strang, G.: A Simple Mesh Generator in MATLAB, SIAM Review, 46, 2004, https://doi.org/10.1137/S0036144503429121, 2004.

Piggott, M. D., Farrell, P. E., Wilson, C. R., Gorman, G. J., and Pain, C. C.: Anisotropic mesh adaptivity for multi-scale ocean modelling, Philosophical Transactions of the Royal Society A: Mathematical, Physical and Engineering Sciences, 367, 4591–4611,
15 https://doi.org/10.1098/rsta.2009.0155, 2009.

Pringle, W. J., Yoneyama, N., and Mori, N.: Multiscale Coupled Three-dimensional Model Analysis of the Tsunami Flow Characteristics around the Kamaishi Bay Offshore Breakwater and Comparisons to a Shallow Water Model, Coastal Engineering Journal, https://doi.org/10.1080/21664250.2018.1484270, 2018.

Register, A. H.: A Guide to MATLAB Object-Orientated Programming, Chapman and Hall/CRC, 2017.

20 Roberts, K. J. and Pringle, W. J.: OceanMesh2D: User guide - Precise distance-based two-dimensional automated mesh generation toolbox intended for coastal ocean/shallow water, https://doi.org/10.13140/RG.2.2.21840.61446/2, 2018.

Shewchuk, J. R.: What Is a Good Linear Finite Element? - Interpolation, Conditioning, Anisotropy, and Quality Measures, Tech. rep., In Proc. of the 11th International Meshing Roundtable, 2002.

Technology Riverside Inc. and AECOM: Mesh Development, Tidal Validation, and Hindcast Skill Asessment of an ADCIRC Model for the
25 Hurricane Storm Surge Operational Forecast System on the US Gulf-Atlantic Coast, Tech. rep., National Oceanic and Atmospheric Administration/Nation Ocean Service, Coast Survey Development Laboratory, Office of Coast Survey, https://doi.org/10.7921/G0MC8X6V, 2015.

Thyng, K. M., Greene, C. A., Hetland, R. D., Zimmerle, H. M., and DiMarco, S. F.: True colors of oceanography: Guidelines for effective and accurate colormap selection, Oceanography, 29, 9–13, https://doi.org/10.5670/oceanog.2016.66, 2016.

30 Wang, Q., Danilov, S., Sidorenko, D., Timmermann, R., Wekerle, C., Wang, X., Jung, T., and Schröter, J.: The Finite Element Sea Ice-Ocean Model (FESOM) v.1.4: formulation of an ocean general circulation model, Geoscientific Model Development, 7, 663–693, https://doi.org/10.5194/gmd-7-663-2014, 2014.

Wessel, P. and Smith, W. H. F.: A global, self-consistent, hierarchical, high-resolution shoreline database, Journal of Geophysical Research: Solid Earth, 101, 8741–8743, https://doi.org/10.1029/96JB00104, 1996.

35 Westerink, J. J., A., L. R., and C., M. J.: Modelling tides in the western North Atlantic using unstructured graded grids, Tellus A, 46, 178–199, https://doi.org/10.1034/j.1600-0870.1994.00007.x, 1994.